CHALMERS

Evaluation of material models in LS-DYNA for impact simulation of white adipose tissue

Master's Thesis in Solid and Fluid Mechanics

KRISTOFER ENGELBREKTSSON

Department of Applied Mechanics
Division of Material and Computational Mechanics and Division of Vehicle Safety
CHALMERS UNIVERSITY OF TECHNOLOGY
Göteborg, Sweden 2011
Master's Thesis 2011:46

MASTER'S THESIS 2011:46

Evaluation of material models in LS-DYNA for impact simulation of white adipose tissue

Master's Thesis in Solid and Fluid Mechanics

KRISTOFER ENGELBREKTSSON

Department of Applied Mechanics
Division of Material and Computational Mechanics and Division of Vehicle Safety
CHALMERS UNIVERSITY OF TECHNOLOGY

Göteborg, Sweden 2011

Evaluation of material models in LS-DYNA for impact simulation of white adipose tissue
KRISTOFER ENGELBREKTSSON

Master's Thesis 2011:46
ISSN 1652-8557
Department of Applied Mechanics
Division of Material and Computational Mechanics and Division of Vehicle Safety
Chalmers University of Technology
SE-412 96 Göteborg
Sweden
Telephone: + 46 (0)31-772 1000

Chalmers Reproservice
Göteborg, Sweden 2011

Evaluation of material models in LS-DYNA for impact simulation of white adipose tissue
Master's Thesis in Solid and Fluid Mechanics
KRISTOFER ENGELBREKTSSON
Department of Applied Mechanics
Division of Material and Computational Mechanics and Division of Vehicle Safety
Chalmers University of Technology

Abstract

Human body models (HBM) are used as tools in crash simulations when investigating the interactions between the human body and the vehicle, thus gaining insight into the evolution of stresses and strains influencing the different parts of the body. In todays crash simulations two broad categories of mathematical HBM are in usage, namely multibody dynamics and finite element. Due to decreasing cost of computational resources there is a shift towards the more biofidelic finite element HBM.

Recent studies have shown correlations between increased risk of death in severe motor vehicle crashes and different categories of obesity, namely the moderately and the morbidly obese. Due to an increasing trend in the obese population there is a need for deeper knowledge and understanding of the constitutive behaviour of the human fat tissue, more specifically the white adipose tissue.

Through a literature study the current research field was explored, and a summary of mechanical properties and available experiments were compiled. It was found that the white adipose tissue behaves as an incompressible solid with nonlinear strain stiffening and nonlinear strain rate stiffening. Further the tissue was found to be isotropic. Unrecoverable deformation was also found to be present in three studies but it was explained in two different manners. One study used plastic deformation and another claimed the tissue hadn't been given enough relaxation time for it to be fully recovered. Three experiments were chosen to be modeled with the Finite Element code LS-DYNA. One experiment was chosen for material model calibration while two experiments were chosen for evaluation. Three material models were chosen for calibration, Ogden Rubber 77 with linear viscoelasticity, Soft Tissue 92 with viscoelasticity and Simplified Rubber 181 with strain rate dependency.

The results of the work reveals a good fit of the Ogden Rubber material model to low and intermediate strain rates. The Soft Tissue material model is less suited to accomodate the nonlinear strain stiffening of the adipose tissue since it is only of order two. The Simplified Rubber material model accomodates the nonlinear strain stiffening as the Ogden Rubber material model but suffers from the drawback of an instant response in the stress to a change in the loading velocity.

The main contribution of the work is two material models that produce a good fit to compressive tests performed at strain rates 0.2/s and 100/s, however, more simulations and tests are needed in order to properly validate the models. The work also contributes with an extensive search through the current research field indicating a paucity of experiments conducted in the high strain rate regime.

Keywords: white adipose tissue, LS-DYNA, material modeling, high strain rate, large strains, finite deformation, viscoelastic, fat

Contents

Aknowledgements

I would like to thank my examiner Karin Brolin and my two supervisors Krystoffer Mroz and Kenneth Runesson for their help during this project. I would also like to thank the people at the division of Material and Computational Mechanics and the division of Vehicle Safety for their help with various questions. Further I would like to thank Bengt Pipkorn at Autoliv for reading and commenting the thesis.

Göteborg August 2011
Kristofer Engelbrektsson

Nomenclature

BAT Brown Adipose Tissue, page 3

FE Finite Element, page 2

HBM Human Body Models, page 2

MRI Magnetic Resonance Imaging, page 5

Ovine Sheep, page 4

Porcine Pig, page 4

WAT White Adipose Tissue, page 2

1 Introduction

Human body models (HBM) are used as a tool in crash simulations when investigating the interactions between the human body and the vehicle thus gaining insight into the evolution of stresses and strains affecting the different parts of the body. In todays crash simulations two broad categories of mathematical HBM are in usage. Due to decreasing cost of computational resources there is a shift towards the more biofidelic finite element HBM. The model contains soft tissues, internal organs, bones, muscles and has the advantage of being able to deliver stresses and strains within tissues. This is advantegous since if the stresses and strains are known inside an organ, failure critera can be set and it is possible to find out if damage has occured inside the organ.

Recent studies have shown correlations between increased risk of death in severe motor vehicle crashes and different categories of obesity, namely the moderately and the morbidly obese [9]. Due to an increasing trend in the obese population there is a need for deeper knowledge and understanding of the constitutive behaviour of the human fat tissue, more specifically the White Adipose Tissue (WAT). Sought for are the dynamic mechanical properties of the tissue since the crash is a very rapid event imposing large accelerations on the body.

The thesis aims at obtaining a validated finite element model of the human WAT suitable for dynamic impact simulation.

1.1 Objectives

- Compilation of properties of fat
- Choose potential material models for fat
- Obtain mechanical test data for validation
- Obtain validated Finite Element(FE)-models of the mechanical tests
- Obtain validated material models

1.2 Limitations

The work is restricted to the compressive range of strain due to a lack of available experiments. Further due to time restrictions the work is limited to obtain a model fitted to compressive strain rates of 0.2/s and 100/s. Since the work considers impact simulation only the loading part will be taken into account neglecting possible hysteresis and unrecoverable deformation.

1.3 Approach

The project starts with a literature study of the properties and structure of the WAT. The output of this literature study will be a list of properties that is going to serve as requirement specification for selection of suitable material models. Further, a literature study of available mechanical tests are to be conducted in order to obtain a foundation for validation of the selected material models. The geometry of the mechanical tests are going to be modeled in the commercial software LS-PrePost[3]. From these geometries meshes will be created, also in the LS-PrePost[3]. Finally the numerical analysis will be conducted in the commercial software LS-Dyna[21].

1.4 The Adipose Organ

In contradiction to common knowledge the fat tissue in the human body is collectively considered an organ. The Adipose organ constitutes several depots located throughout the human body. Firstly, the depots are divided into visceral and subcutaneous WAT as can be seen in figure 1.1. These broad categories are further divided into intraperitoneal and retroperitoneal respectively superficial subcutaneous WAT and deep subcutaneous WAT. The Intraperitoneal depot is then divided into the omental and mesenteric depot[6]. All above depots contain the WAT and Brown Adipose Tissue(BAT). The WAT has an energy storage function whereas BAT is used for thermogenesis. In adults there exist a relatively little amount of BAT compared to WAT[1]. The major part of the WAT is found in the omental and mesenteric depots and the subcutaneous depot[6][17].

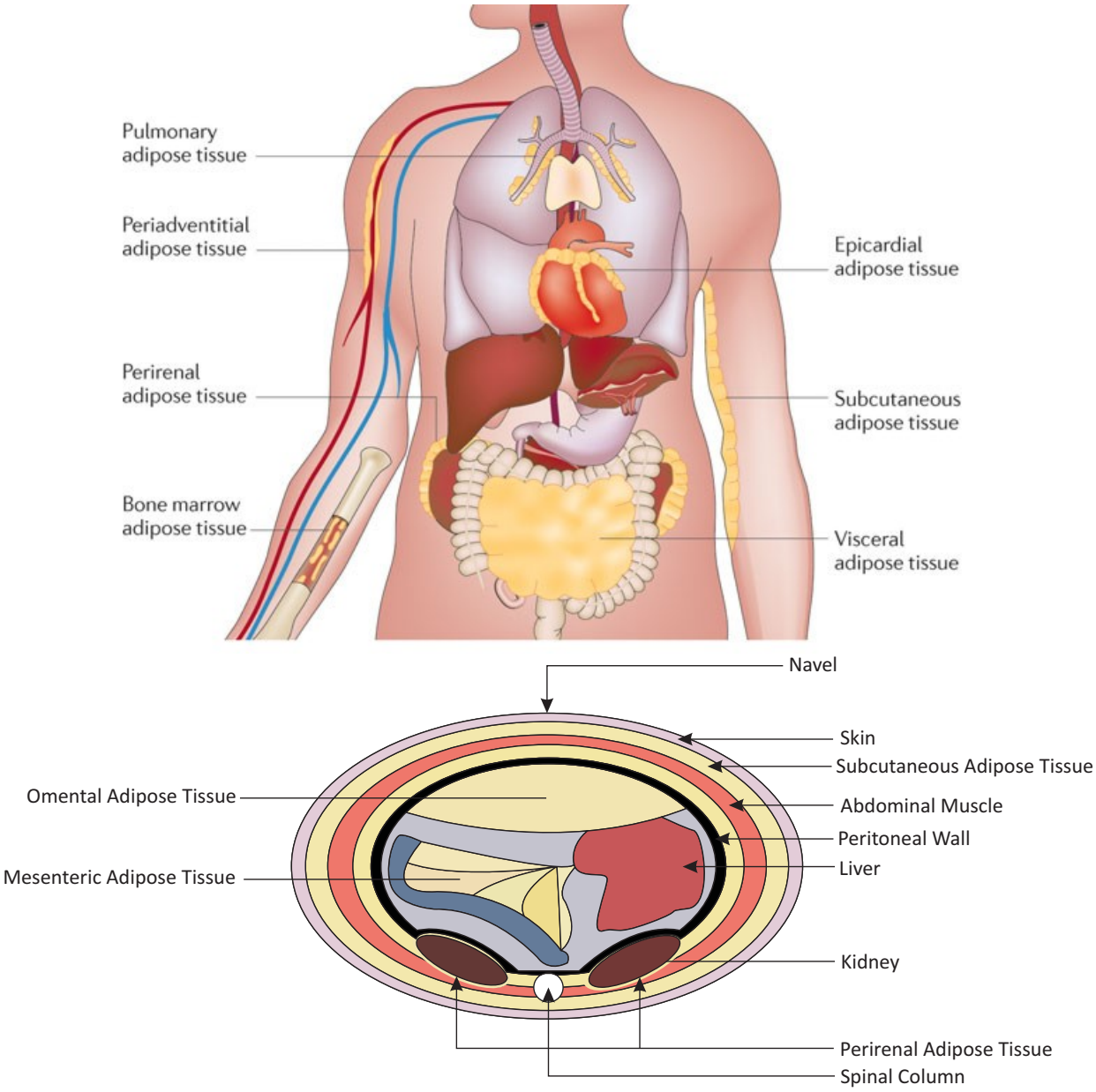

Figure 1.1: Upper: Depot sites of WAT, tissue taken from [18] Lower: Section at navel redrawn from [24]

1.5 Microstructure of WAT

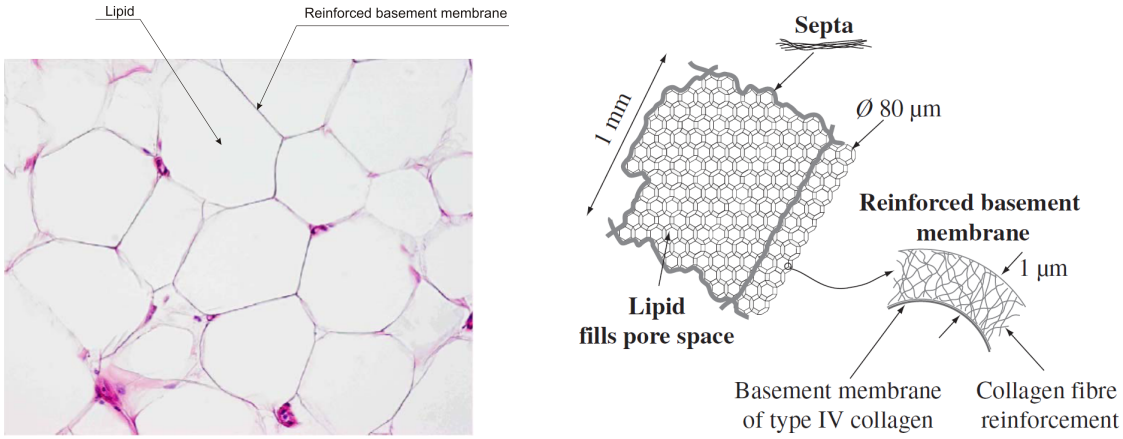

Figure 1.2: Left: Light microscopy. Haematoxylin–eosin staining. Human WAT. Objective magnification 20x. Taken from [1] Right: Schematic of WAT, taken from [2]

The structure of the WAT at cellular level can be seen in figure 1.2. The white adipocyte is the cell containing the lipid droplet and has an approximate diameter of 80 μm. The cell wall consist of a collagen based reinforced basement membrane. At an higher level there exist an open-cell foam like structure called the interlobular septa which contain adipocyte cells and is about 1mm in size. The Septa structure consists of type I collagen[2].

Since the mechanical properties are dependent on the morphology of the tissue it is necessary, when modeling the depot sites, to take into account how large the variations are and due to what factors. Factors such as obesity, age, gender, genetics, various deseases, could be factors that influence the microscopical structure. Further if there are large variations within depot sites this will be considered as inhomogeneity and adds a considerable amount of complexity to the constitutive modeling.

Due to ethical, immunological and supply it is considerably more complicated to obtain human WAT in comparison to an animal model, such as porcine or ovine. If a mechanically similar animal model is found this is obviously preferred to a human subject.

1.6 Mechanical properties of WAT

There are only a few studies available that have investigated mechanical properties of WAT and even less that have taken into account high strain rates in combination with large strains.

Property	Study
Nonlinear stress strain dependency	[13],[7],[4],[15]
Nonlinear dependence of stress on strain rate	[13],[11]
Incompressible	[13]
Isotropic	[13]
Symmetric between tension and compression	[13]
Unrecoverable deformation	[7],[19]

Table 1.1: Table of material properties

The studies are almost always composed of several different types of tests and the strains and strain rates reported in table 1.3 are for the tests with the highest strain and strain rate simultaneously. Below, follows a short summary on the tests in table 1.3 and what material behaviour that emerges from these tests.

Material parameter	Value	Study
Density	925-970 kg/m^3	[16]
Density	920 kg/m^3	[13]
Bulk modulus	0.5 GPa	[13]

Table 1.2: Table of material parameters

There is only one study available considering large strains in combination with large deformation rates [13]. The study reports a nonlinear dependency between stress and strain and a nonlinear dependency upon strain rate. The study succeeded in fitting a one term Ogden hyperelastic model to three different areas of strain rate without any viscoelastic modeling or modeling of the rate dependency. On the other hand the study reported that the shape of the nonlinear stress strain curve is invariant to strain rate and the stress level is consequently governed only by the shear modulus and not the strain hardening parameter[13] Since this study is the only one available suitable for the purpose of impact simulation it is choosen as a basis on which the model in this study is going to be calibrated. Further the study assumes incompressibility due to large liquid content and this is confirmed by an elastic shear modulus of approximately G'=E'/3. This also confirms isotropicity according to [13].

In the test [7] hyperelastic and viscoelastic parameters are obtained by the use of (MRI) and inverse finite element method using indentation testing on exvivo porcine specimens. This study shows that there is unrecoverable deformation after the specimen has been unloaded which according to them would indicate elastoplastic behaviour.

In the test [4] indentation testing is again used, this time on excised breast tissue. The study obtains hyperelastic parameters through inverse finite element method and reveals nonlinear stress strain dependency.

[15] investigates possible thixo- and anti-thixotropy of the WAT through shearing of specimens in a rotational rheometer. They argue that the WAT is able to fully recover if it is given sufficient time.

[5] in a more recent study, the most extensive yet found w.r.t. the number of samples, uses indentation testing and inverse finite element analysis on breast tissue. This time the indentation is performed with a smaller amplitude which is not in a favourable direction for the modeling of large strains. This work is a continuation on their earlier work.

[8] uses the Ovine model instead of the porcine with the argument that it is a popular orthopaedic model. They use indentation testing together with hayes solution to obtain a value of the elastic modulus. This test uses a larger specimen than the other studies and a relatively high indentation speed. However there are no reported values on the force from zero to four millimeter penetration only the value at full penetration.

In the study [19] a rhotational rheometer is used and the complex modulus is obtained. The study concludes that WAT viscosity increases with increasing strain rate indicating shear thinning.

Since the working range of the model includes high strain rates it is reasonable to assume the importance of inertia forces thus a value of the density is needed. There are only a few values in the literature reporting a value of the density of human WAT and the one adopted here is taken from a study performed on six . The study reports a variation of 925-970 kg/m^3 over the whole body[16].

Soft tissues does normally not have symmetric behaviour in tension and compression often due to collagen fibers distributed throughout the tissue. The collagen fibers are assumed incapable of resisting compressive forces therefore yielding different response in tension and compression. However in the case of the WAT [13] reports a symmetry between

Study	Nr. test subjects	Specimen size (mm)	Specie	Analog loc.	Strain	Strain rate	Test type
[13]Comley	20 sa.	r=5, t=8, t=3	Porcine	xx	0-0.4	0.002-5000	Unconfined compression
[7]Sims	6 sa.	irregular approx. r=5	Porcine	xx	xx	xx	Indentation
[4]Samani	2 su. 2 sa.	15x15x10	Human	Breast	(1 mm indent.)	(1 mm/s)	Indentation
[15]Geerligs	(3,3)	r=4, t=1.5	Porcine	DSA	0-0.15	0.01-1	Torsion
[5]Samani	71 sa. 71 su.	15x15x10	Human	Breast(WAT)	(0.5 mm indent.)	(0.5 mm/s)	Indentation
[8]Gefen	10 sa. 10 su.	r=30 t=45	Ovine	xx	(4 mm indent.)	(2000 mm/s)	Indentation
[19]Patel	6 sa./test	xx	human	SA	0.1-0.2	0.1-15rad/s	Torsion

Table 1.3: Summary of found experiments, sa. = samples, su. = subjects. The xx in column Analog loc. means that there is no similar human depot documented. The xx found in other columns means no information available

tension and compression and non that opposes this have been found. This is obviously not a proof of symmetry since the nonexistence of studies that opposes tensile compressive symmetry is due to lack of studies not extensive testing.

In summary what is sought for is a material model in LS-DYNA able to accomodate the properties in table 1.1, except for the properties that are excluded according to section 1.2.

2 Viscoelasticity

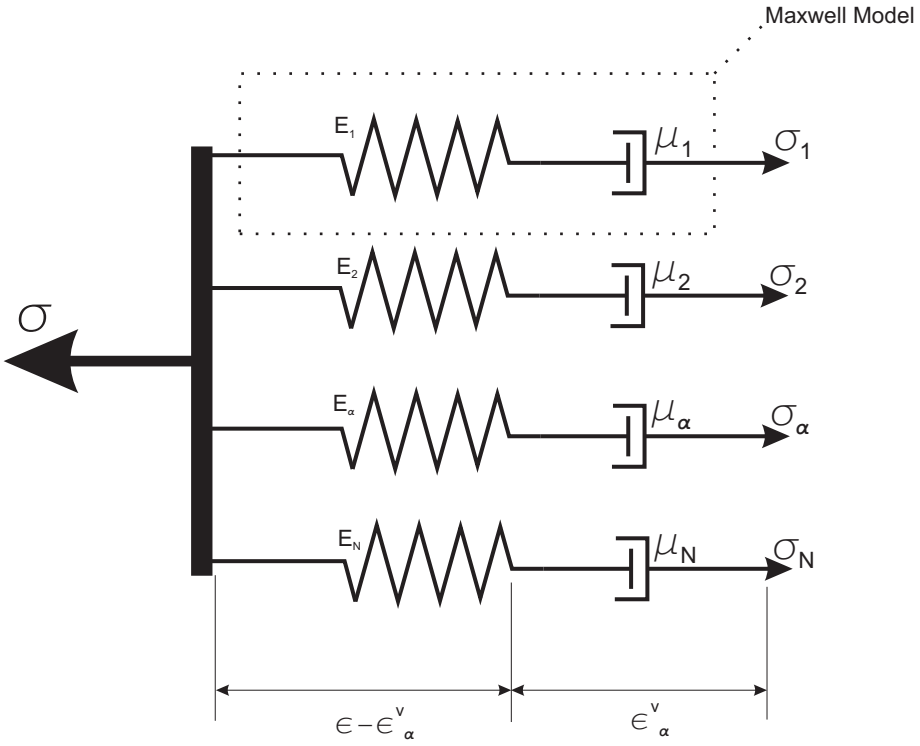

Figure 2.1: Standard Linear Model

This is the Standard Linear Model or otherwise named Generalized Maxwell Model. It can represent solid behaviour if for example $\mu_1 = \infty$ which means that it relaxes towards the value of $\sigma = E_1\epsilon$. The Maxwell model in the dashed region in the figure above represents a fluid since when stretched infinitesimaly there is no resistance. The following derivation is in line with [22]. By looking at the single Maxwell element in the dashed region, free from the above structure, the following is obtained

$$\sigma_1^v = \sigma_1^e = \sigma \tag{2.1}$$

$$\epsilon_1^v + \epsilon_1^e = \epsilon \tag{2.2}$$

This results in, for the single maxwell element

$$\sigma = E_1(\epsilon - \epsilon_1^v) \tag{2.3}$$

There is now one equation but two unknowns since the strain in the damper is not known. The evolution equation for the strain in the damper is introduced

$$\dot{\epsilon}_1^v = \frac{1}{\mu_1}\sigma_1^v \tag{2.4}$$

Since $\sigma_1^v = \sigma$ this results in

$$\dot{\epsilon}_1^v = \frac{1}{\mu_1}E_1(\epsilon - \epsilon_1^v) \tag{2.5}$$

This differential equation can be solved for ϵ_1^v with the appropriate initial condition of $\epsilon_1^v(0) = 0$

Now an arbitrary number of Maxwell elements are added in parallell according to the figure above which by equilibrium yields

$$\sigma = \sum_{\alpha=1}^{N}\sigma_\alpha = \sum_{\alpha=1}^{N}E_\alpha(\epsilon - \epsilon_\alpha^v) \tag{2.6}$$

Further the evolution equation becomes

$$\dot{\epsilon}_\alpha^v = \frac{1}{\mu_\alpha}\sigma_\alpha^v \tag{2.7}$$

By use of $\sigma_\alpha = \sigma_\alpha^v$ and insertion of σ_α from equation (2.6) in equation (2.7) this results in

$$\dot{\epsilon}_\alpha^v = \frac{1}{\mu_\alpha}E_\alpha(\epsilon - \epsilon_\alpha^v) \tag{2.8}$$

Since the above expression is uncoupled it can be solved separately for ϵ_α^v resulting in, for a prescribed constant strain of ϵ_0

$$\epsilon_\alpha^v(t) = \epsilon_0(1 - e^{\frac{-t}{t_{*\alpha}}}) \tag{2.9}$$

Insertion of this equation into equation (2.6) results in

$$\sigma(t) = \underbrace{(\sum_{\alpha=1}^{n}E_\alpha e^{\frac{-t}{t_{*\alpha}}})}_{Pronyseries}\epsilon_0 \tag{2.10}$$

If this is going to be used with a variable prescribed strain instead of a constant strain the hereditary formulation can be used

$$d\sigma(t,\tau) = R(t-\tau)d\epsilon(\tau) = R(t-\tau)\frac{d\epsilon(\tau)}{d\tau}d\tau \tag{2.11}$$

Summing this by integration from 0 to t results in

$$\sigma(t) = \int_0^t R(t-\tau)\frac{d\epsilon(\tau)}{d\tau}d\tau \tag{2.12}$$

Insertion of the Prony series results in

$$\sigma(t) = \int_0^t (\sum_{\alpha=1}^{n}E_\alpha e^{\frac{-(t-\tau)}{t_{*\alpha}}})\frac{d\epsilon(\tau)}{d\tau}d\tau \tag{2.13}$$

That is the Prony series is actually a collection of Maxwell elements in parallel. If, for example, two terms are used then two hereditary integrals are obtained where the relaxation function of each is a Maxwell element.

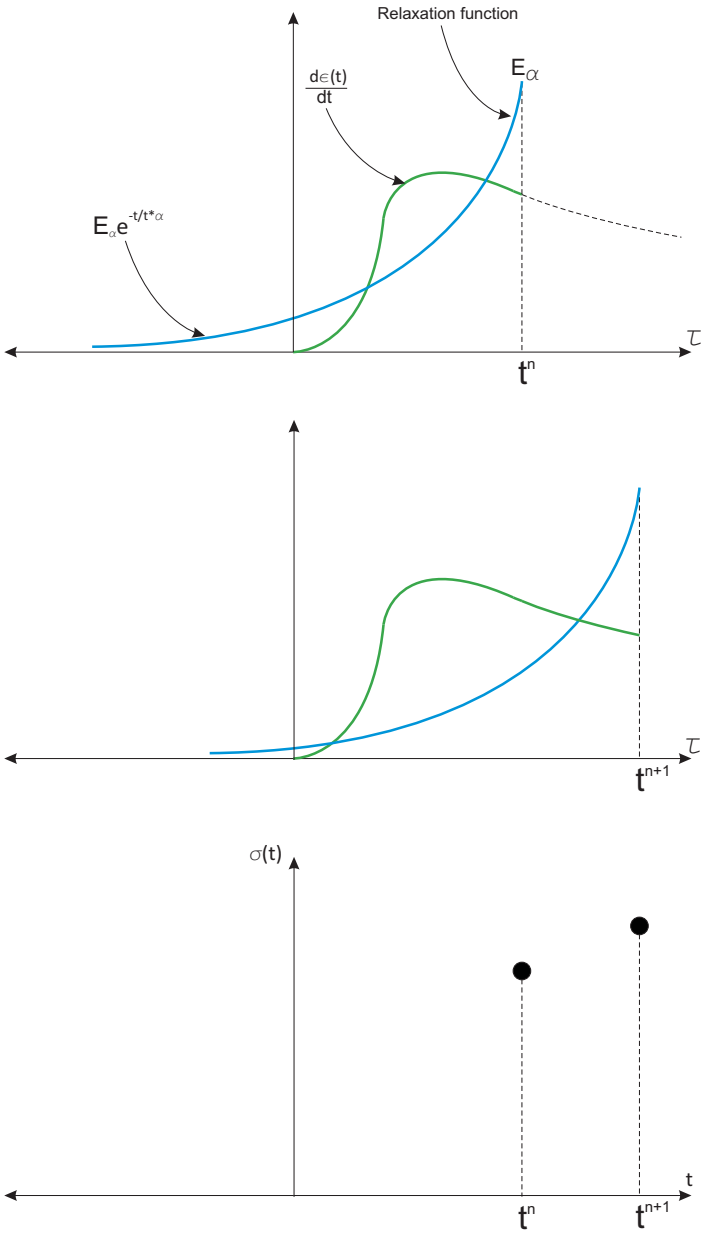

Figure 2.2: Convolution of one term Prony series with strain rate

Figure 2.2 shows graphically how the hereditary integral with one element in the prony serie is calculated, that is equation (2.13) with n=1. The value of $\sigma(t)$ at t^n is calculated as the integral of the product of the blue and green line. This gives the material model a fading memory where a certain strain rate at an earlier time influence the stress at current time less and less. This fading property is determined by the relaxation time t*. The larger the t* the slower the exponential function asymptotically approaches zero. If for example three terms are used in the prony serie three of these integrals are obtain where it is possible for each to have its own $t*_\alpha$ and E_α.

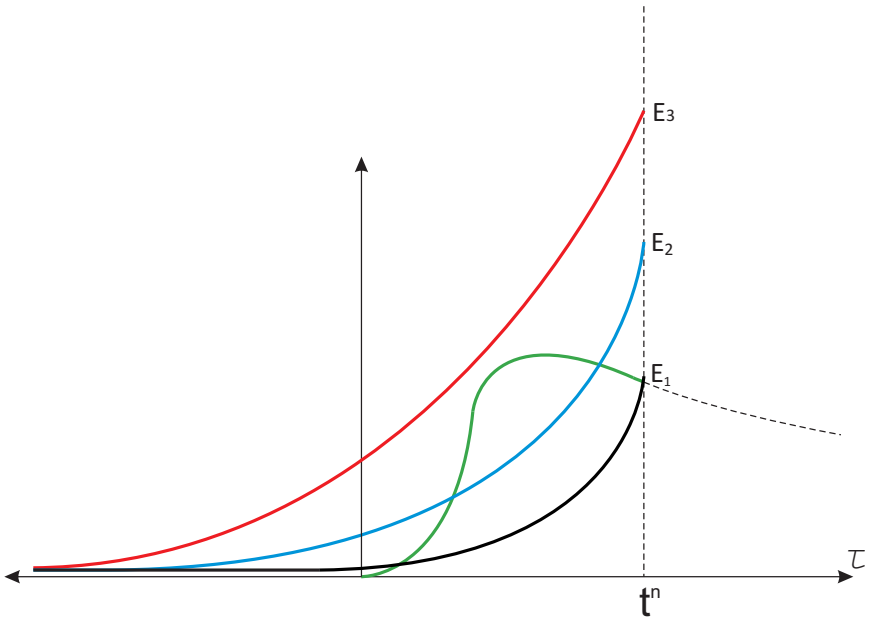

Figure 2.3: Convolution of three term Prony series with strain rate

In figure 2.3 the three exponential curves are added then the integral of the product of the new curve with the strainrate gives the stress at t^n

3 Available models in LS DYNA

LS-Dyna[21] has a vast selection of possible choices for a material model however for this particular material only a handful seems reasonable at first sight. Material models suitable for a more indepth study has been choosen based on the criteria in section 1.6. The information in this section is taken from [20],[21] unless another source is explicitly cited.

Name	Model nr.
Soft tissue	92
Simplified Rubber	181
Ogden rubber	77O
Viscoelastic(For reference, THUMS)	006

3.0.1 Soft tissue

This model is a transversely isotropic model in tension and isotropic in compression with the strain energy function in the equation below. The reason for investigating this model further even though it opposes the symmetric tensile compressive and isotropic behaviour of the WAT is if it is possible to adjust parameters in order become isotropic and symmetric in tension and compression.

$$W = \underbrace{C_1(\tilde{I}_1 - 3) + C_2(\tilde{I}_2 - 3)}_{MooneyRivlin} + F(\lambda) + \frac{1}{2}K(ln(J))^2 \tag{3.1}$$

$$\frac{\partial F}{\partial \lambda} = \left\{ \begin{array}{cc} 0 & \lambda < 1 \\ \frac{C_3}{\lambda}[exp(C_4(\lambda - 1)) - 1] & \lambda < \lambda^* \\ \frac{1}{\lambda}(C_5\lambda + C_6) & \lambda \geq \lambda^* \end{array} \right\}$$

As can be seen in equation (3.0.1) it is possible to obtain only the mooney rivlin solid by setting the value of C_3 and C_4 to zero and letting λ^* being large enough so that it is never reached.

The viscoelastic contribution is on the following form

$$\mathbf{S}(\mathbf{C},t) = \mathbf{S}^{\mathbf{e}}(\mathbf{C}) + \int_0^t 2G(t-s)\frac{\partial W}{\partial \mathbf{C}(s)}ds \tag{3.2}$$

And with the prony serie inserted in the above equation

$$\mathbf{S}(\mathbf{C},t) = \mathbf{S}^{\mathbf{e}}(\mathbf{C}) + \int_0^t 2(\sum_{i=1}^{6} S_i e^{\frac{t-s}{T_i}})\frac{\partial W}{\partial \mathbf{C}(s)}ds \tag{3.3}$$

3.0.2 Simplified rubber

This model is a tabulated version of the Ogden model described previously. It has the advantage that no parameter fitting is necessary since it directly uses uniaxial stress strain curves obtained from experiments in order to calculate the stresses. There is no viscoelasticity in this model, instead, the model uses stress strain curves from experiments performed at different strain rates. If for example two curves are used all values of stress at a particular strain and strainrate will be a linear interpolation between the two curves. A drawback of this approach to the strainrate dependency is that change in the loading velocity will give an immediate respose[10]. An advantage on the other hand is that the shape of the curves at different strainrates can have whatever shape since they are defined by the tabulated values. That is there is no need for adjusting parameters in order to accomodate a specific shape of the stress-strain curve at a particular strainrate, the tabulated curve is used instead.

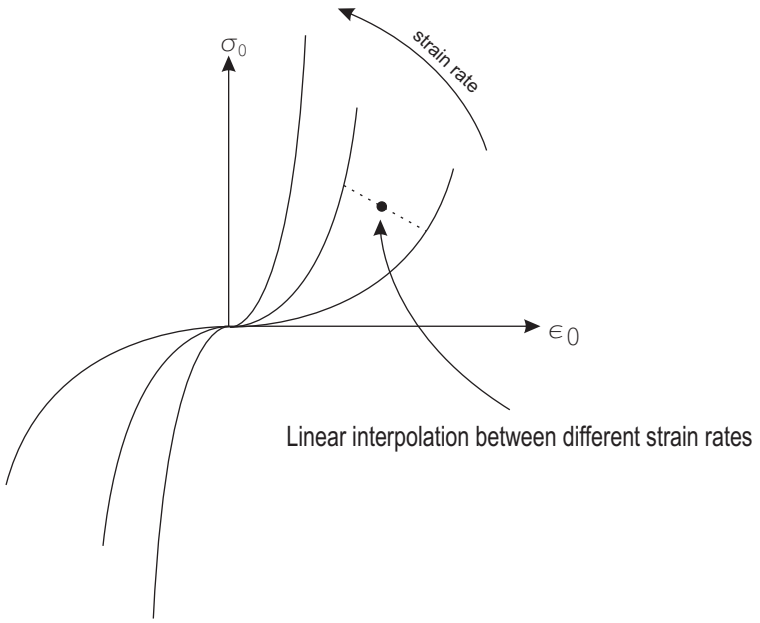

Figure 3.1: Engineering stress versus engineering strain for different strainrates used as input in the model simplified rubber

3.0.3 Ogden rubber

This model is a hyperelastic nearly incompressible model in principal directions with the following expression for the free energy.

$$\Psi = \sum_{i=1}^{3}\sum_{j=1}^{n}\frac{\mu_j}{\alpha_j}(\lambda_i^{\hat{\alpha}_j} - 1) + K(J - 1 - lnJ) \tag{3.4}$$

After some calculations and using only one term in the innermost sum above the expression for the second Piola Kirchhoff stress is obtained as

$$\mathbf{S} = \sum_{i=1}^{3}(\mu(\hat{\lambda}_i^{\alpha} - \frac{1}{3}(\hat{\lambda}_1^{\alpha} + \hat{\lambda}_2^{\alpha} + \hat{\lambda}_3^{\alpha}))) + KJ(J-1)(\mathbf{F}^{-1}\mathbf{n}_i) \otimes (\mathbf{F}^{-1}\mathbf{n}_i) \tag{3.5}$$

In addition to this hyperelastic model there is a viscoelastic contribution in the following form

$$S_{ij} = \int_0^t G_{ijkl}(t-\tau)\frac{\partial E_{kl}}{\partial \tau}d\tau \tag{3.6}$$

This viscoelastic stress is then added to the stress determined from the ogden model above resulting in

$$\mathbf{S} = \sum_{i=1}^{3}(\mu(\hat{\lambda}_i^{\alpha} - \frac{1}{3}(\hat{\lambda}_1^{\alpha} + \hat{\lambda}_2^{\alpha} + \hat{\lambda}_3^{\alpha}))) + KJ(J-1)(\mathbf{F}^{-1}\mathbf{n}_i) \otimes (\mathbf{F}^{-1}\mathbf{n}_i) + \int_0^t G_{ijkl}(t-\tau)\frac{\partial E_{kl}}{\partial \tau}d\tau \tag{3.7}$$

3.0.4 Viscoelastic

There will be no detailed description on the viscoelastic model since it is only used for comparison. The viscoelastic model in LS DYNA is used in the Total Human Model for Safety(THUMS)(Toyota corporation) HBM, when modeling soft tissues. It is not specifically used for WAT but for soft tissues in general hence care needs to be taken when using this model for comparison.

4 Method

In the FE-modelling part of the thesis the commercial solver LS-DYNA(version: ls971s R5.1.1)[21] have been used together with the Pre/Post tool LS-Pre-Post [3]. LS-DYNA[21] is primarily an explicit FE-code. This has the advantage of less demanding timestep calculation than the implicit time integration since the inverse of the stiffness matrix does not need to be calculated. This is advantageous in short physical time analysis such as impact simulation. The drawback of the method is that it is conditionally stable since the stability depends on the timestep being short enough to capture an elastic wave at the speed of sound of the material being used. That is the timesstep depends on the shortest element side length and the speed of sound $c = \sqrt{\frac{K}{\rho}}$. The previous expression for the speed of sound is a one dimensional expression and the timestep actually depends on the highest eigenfrequency of the structure however this simple formula is sufficient to keep in mind to get a feeling of in which direction the timestep size will go if the density or the bulk modulus is changed. Dynamic implicit time integration with the Newmark method is

used when the simulation approaches the quasistatic case. For the extraction of data from figures in the test studies the commercial software Matlab have been used.

4.1 Experiments

The chosen experiments are presented beginning, with the test used for material model calibration [13] in 4.1.1. Proceeding, with an indentation experiment on WAT [8] in 4.1.2 used for evaluation of behaviour at higher velocities. Finally, a torsion experiment on WAT [15] in 4.1.3 used for evaluation of material model shear behaviour.

4.1.1 Calibration

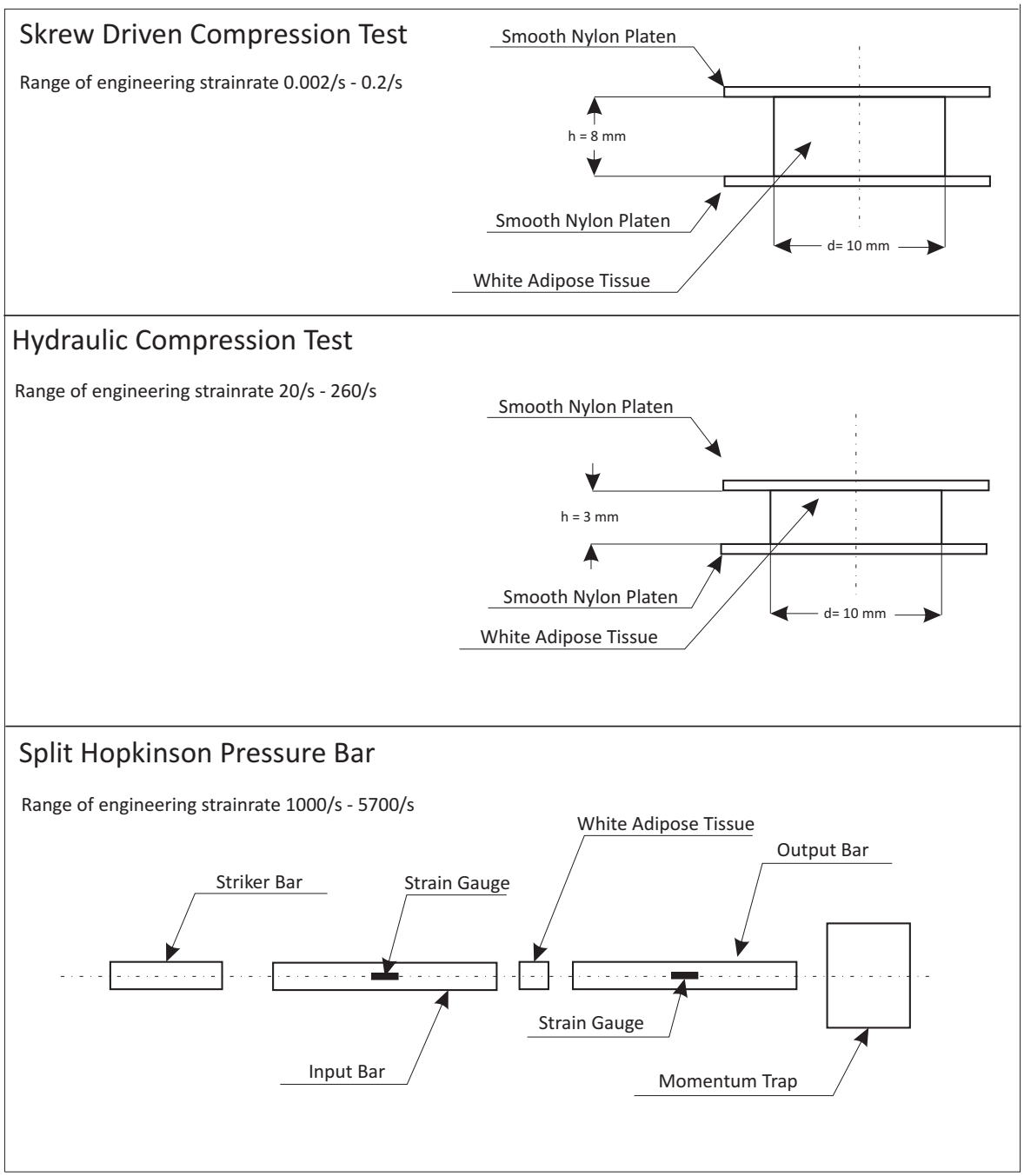

Figure 4.1: Unconfined compression experiments [13]

In figure 4.1 experiment [13] is summarized. This experiment was chosen based on the large strains and high strain rates investigated. The test is divided into three different parts where three different test-methods have been used for three different ranges of strain-rate. The experiment was performed at three different levels of strain rate in unconfined compression.

At low strain rate a skrew driven compression test machine was used and the data was measured by a 5N load cell with a sensitivity of 20 mN within 1%. The specimen was compressed between two nylon platens with a thickness of 15 mm. In figure 4.2 the result of the skrew driven compression test is shown. The curve at 0.2/s is chosen for comparison with the later developed FE-model. The reason for choosing only one curve is that there is not always a continous increasing stiffness from lower to higher strain rates within the levels, low, intermediate and high strain rate, hence one curve is sufficient. More curves would not increase the accuracy.

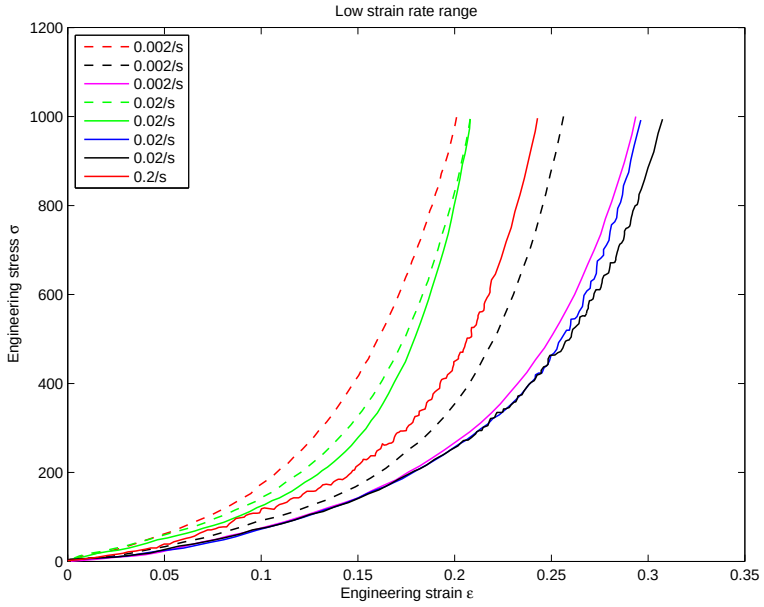

Figure 4.2: Skrew driven compression test [13]

In the intermediate strain rate range a servohydraulic compression test machine was used. Again the specimens were compressed between nylon platens. Further a load cell was used consisting of an aluminum beam with four Wheatsone bridges. The dimensions of the load cell was not specified and it was not possible to obtain the blueprints. The impacting platen was accelerated up to the required velocity before impacting the specimen. In figure 4.3 the result of the hydraulic compression test is shown. The curve at 100/s is chosen for comparison with the later developed FE-model. The reason again for choosing only one curve is the same as for the low level strain rate.

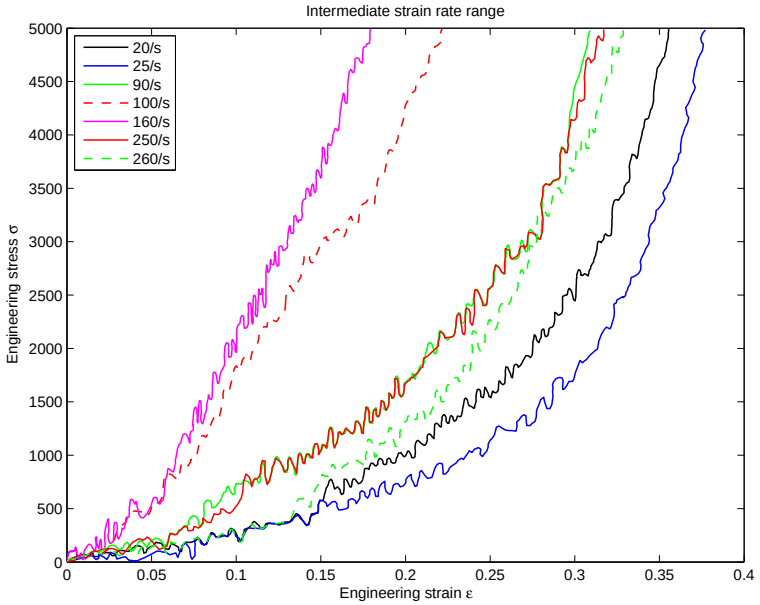

Figure 4.3: Hydraulic compression test [13]

In the high strain rate region the method is changed to the split hopkinson pressure bar method. The striker bar is impacted into the input bar creating an elastic wavefront. The wavefront transmitts into the specimen and further into the output bar. An elastic wave is also reflected at each boundary. These strains are then measured by the strain gauges and then a calculation is performed yielding the stress strain response in the specimen [13]. In figure 4.4 the result of the split hopkinson pressure bar is shown. These curves are shown for completeness and this range of strain rate will not be modeled.

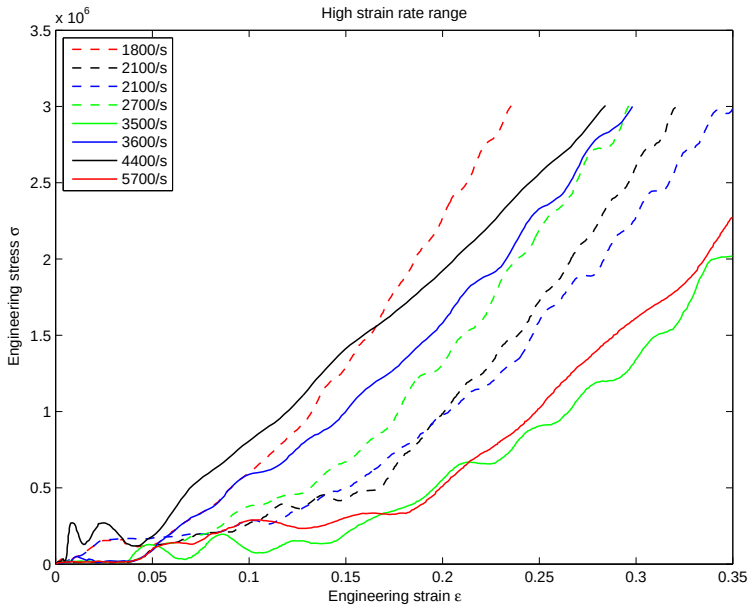

Figure 4.4: Split hopkinson pressure bar [13]

4.1.2 Evaluation 1

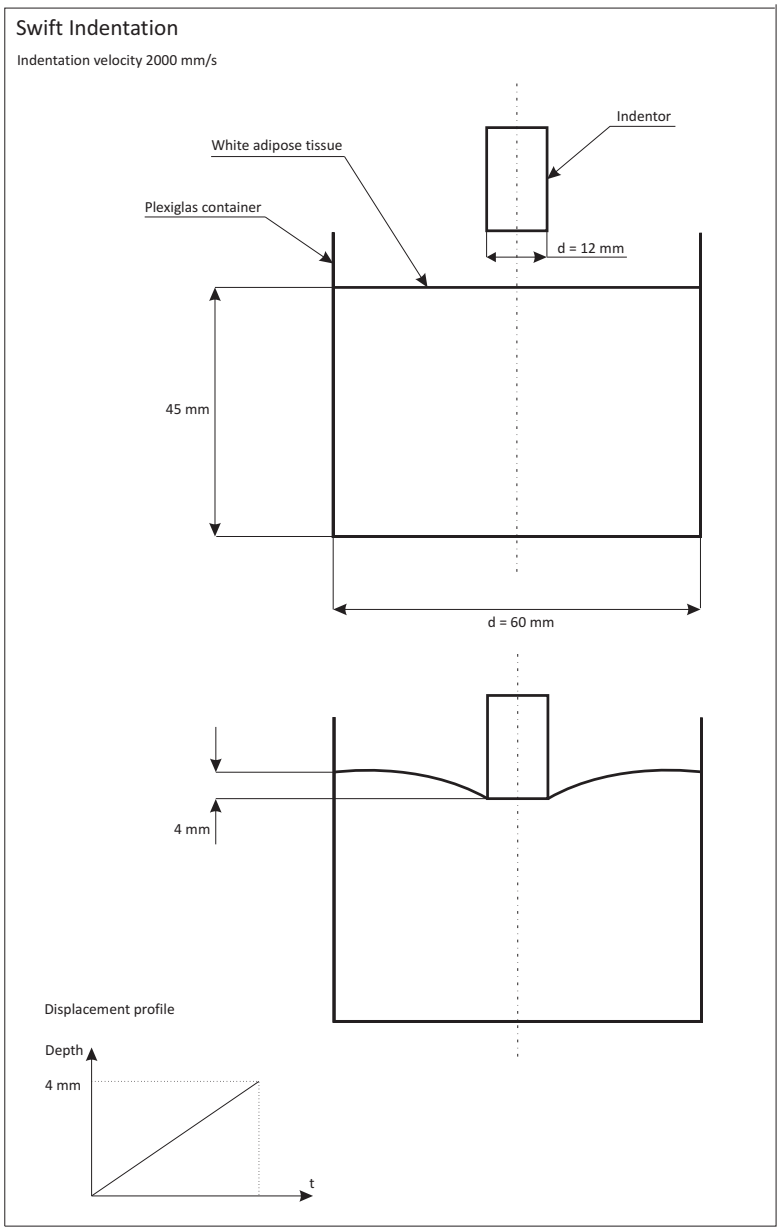

Figure 4.5: Swift indentation [8]

In the first evaluation experiment [8] in figure 4.5 a pneumatically driven piston of 12 mm diameter is indented into a specimen of ovine WAT. The specimen is contained in a plastic cylinder. The force in the indentor is measured at a penetration depth of 4 mm. The result from [8] can be seen in table 4.1. The value in the eighth cycle is used for later comparison.

	Cycle 1	Cycle 2	Cycle 3	Cycle 4	Cycle 5	Cycle 6	Cycle 7	Cycle 8
Mean Peak force (N)	13.3587	10.0279	9.8759	9.6057	9.6406	8.7956	8.9233	8.5679
Standard deviation peak force (N)	6.1064	6.1330	5.7758	5.6079	5.8681	5.0864	5.2437	5.1378

Table 4.1: Peak force at 4 mm penetration. Mean value consists of 10 samples. Taken from [8]

4.1.3 Evaluation 2

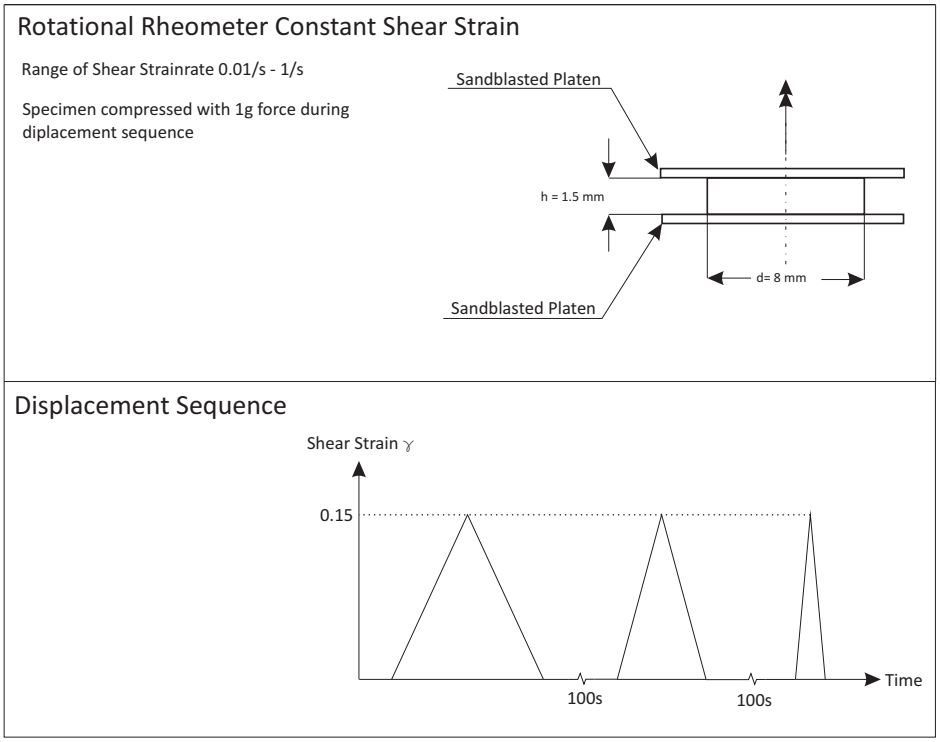

Figure 4.6: Constant shear strain experiment [15]

The evaluation 2 experiment [15] is summarized in figure 4.6. The testing device used was a rotational rheometer (Ares, Rheometric Scientific, USA) with sandblasted parallell plates. A slight compression of 1 gram was exerted on the specimen throughout the displacement sequence in order to increase the friction between the plates. Then a load and unloading sequence was performed with a rest interval of 100 s between each load unloading cycle. The shear strain rate was increased with every cycle beginning at 0.01/s, proceeding with 0.1/s and finally performed at 1/s.

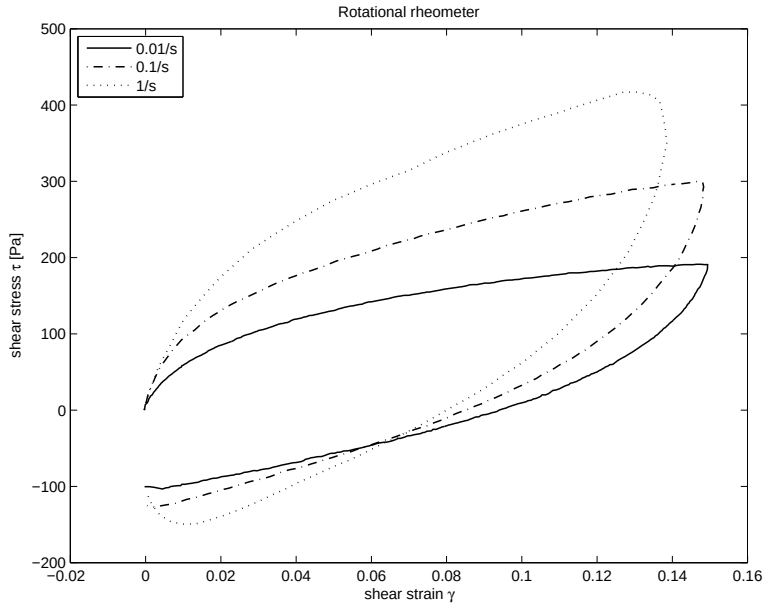

Figure 4.7: Constant shear strain experiment with increasing strain rate [15]

In figure 4.7 the result of the experiment is displayed. Only the loading part of these curves will be used for comparison according to the limitations of this thesis.

4.2 Mesh and Boundary Conditions

In this subsection the actual mathematical modelling of the three chosen experiments are presented. Beginning, with modelling of the calibration experiment [13] in 4.2.1. Proceeding, with modelling of evaluation 1 experiment [8] in 4.2.2. Finally, the modelling of evaluation 2 experiment [15] in 4.2.3.

4.2.1 Modelling Calibration

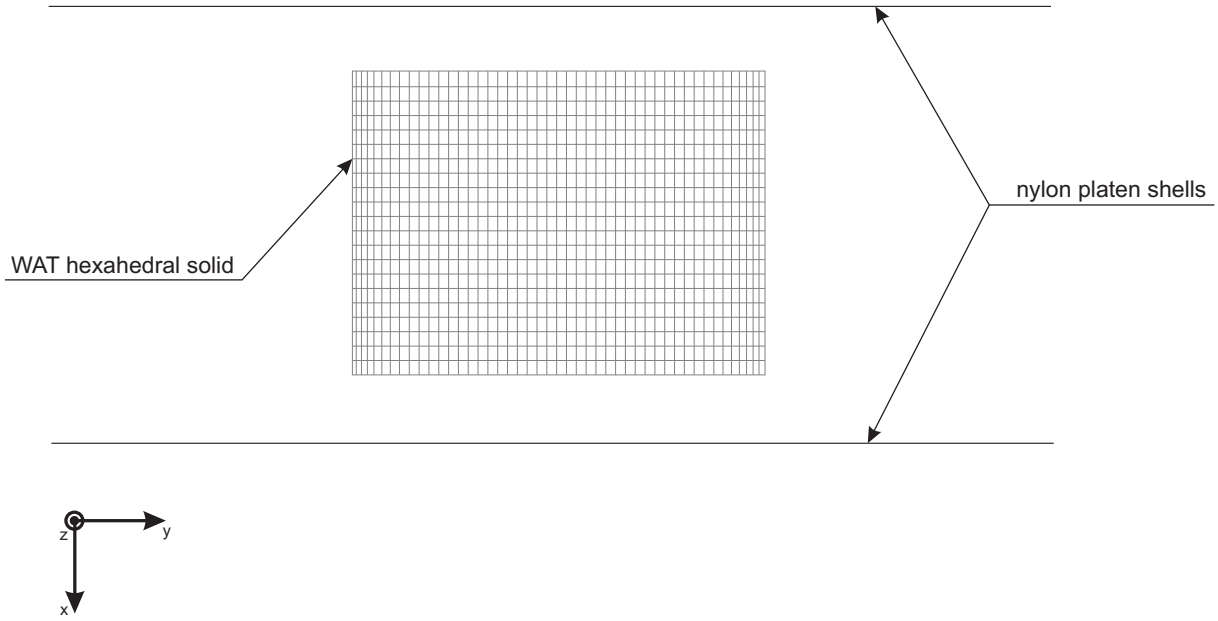

Figure 4.8: Hexahedral mesh for the skrew driven unconfined compression test

The hexahedral mesh used to simulate the skrew driven compression test [13] is shown in figure 4.8. The upper nylon platen shell is displaced in the x-direction and the lower nylon plate shell is locked in all directions. The WAT hexahedral mesh rests on the contact formulations. An adequate mesh density of 600 hexahedrons have been established through the convergence study in appendix B. Allthough the convergence study was performed at 100/s it is assumed that this mesh density is sufficient also for the test at strain rate 0.2/s. The shells are covered with nullshells which are present in order to facilitate contact calculations and does not contribute to the stiffness calculations. The friction between the platens and the WAT has been modeled with a Coloumb friction formulation where the dynamic and static yield forces have been input. In order to determine reasonable values of the friction, a sensitivity analysis between compression force and friction has been conducted in appendix E.

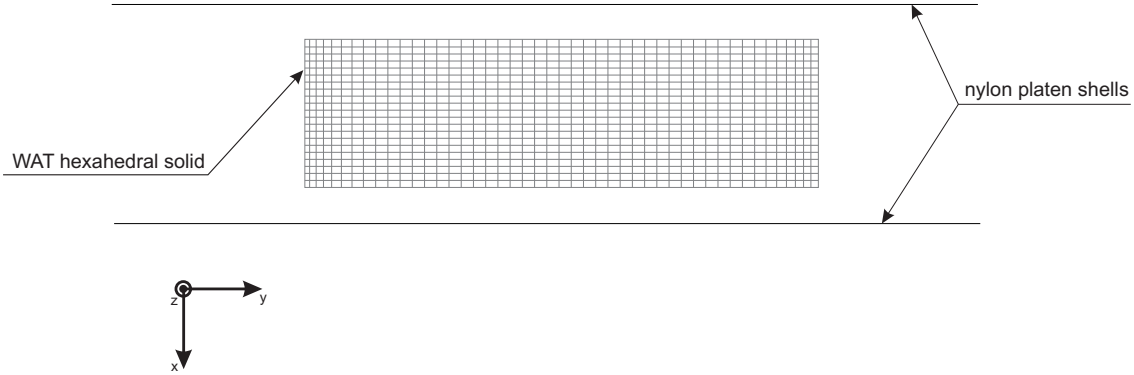

Figure 4.9: Hexahedral mesh the hydraulic unconfined compression test

The hexahedral mesh used to simulate the hydraulic unconfined compression test [13] is shown in figure 4.9. The upper nylon platen shell is displaced in the x-direction and locked in all other directions. The lower nylon platen shell is locked in all directions. The WAT hexahedral mesh rests on the contact formulations. The shells are again covered with nullshells in order to facilitate the contact implementation. The velocityprofile is shown

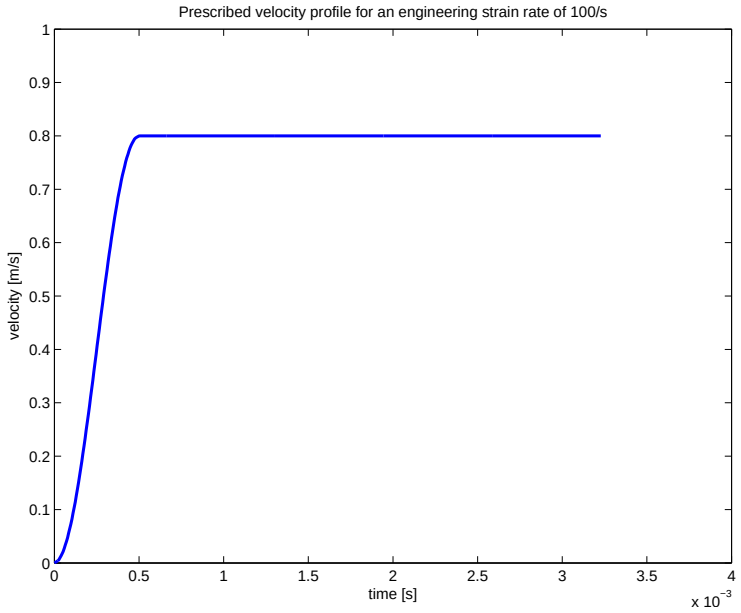

Figure 4.10: Velocity profile with maximimum engineering strainrate 100/s and peak acceleration 2400 m/s^2

in figure 4.10. The risetime of the velocity is choosen long enough not to cause numerical instability and short enough so that constant engineering strainrate is held for the major part of the analysis. It should be noted that the exact velocityprofile is with a very fast acceleration in the beginning due to the platen impacting on the specimen with constant velocity.

4.2.2 Modelling Evaluation 1

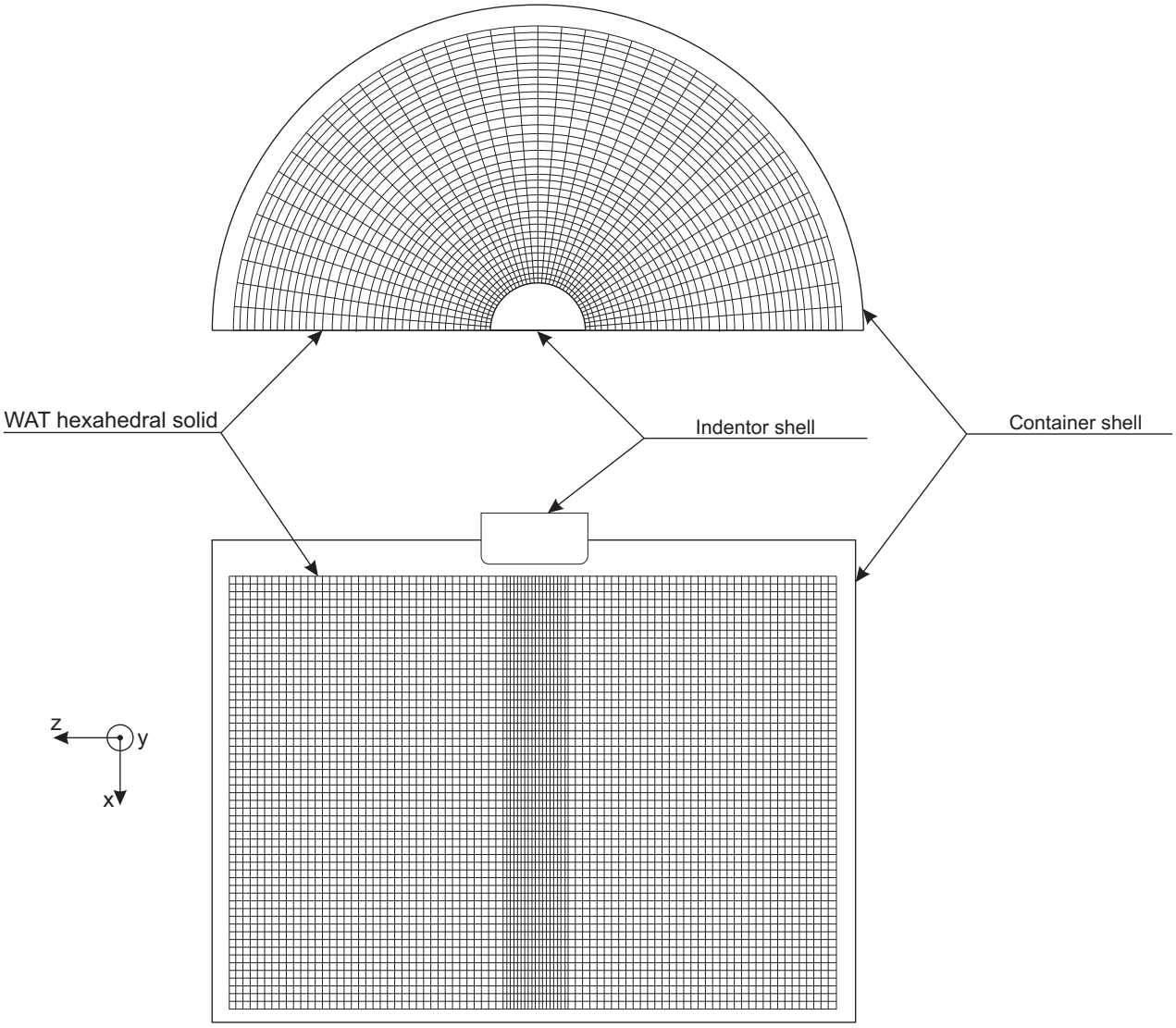

Figure 4.11: Hexahedral mesh of evaluation 1

The mesh used to simulate the evaluation 1 experiment [8] is shown in figure 4.11. The indentor is placed half the shell thickness away from the WAT in order for it to be in contact from the beginning. The indentor shell is then accelerated upto a constant velocity of 2000 mm/s and then stopped at 4 mm penetration where the force is. The container is represented by a shell. Note that there are small elements, not visible in figure, on the shells of the indentor and plastic cylinder which does not slow down the calculation since they are assigned ridgid material properties. The container shell is locked in all degrees of freedom and the WAT rests inside on the contact formulation between the shell and the WAT. The friction between the different parts is the coefficients established in appendix E. It is assumed that these coefficients would be the same as in the calibration.

4.2.3 Modelling Evaluation 2

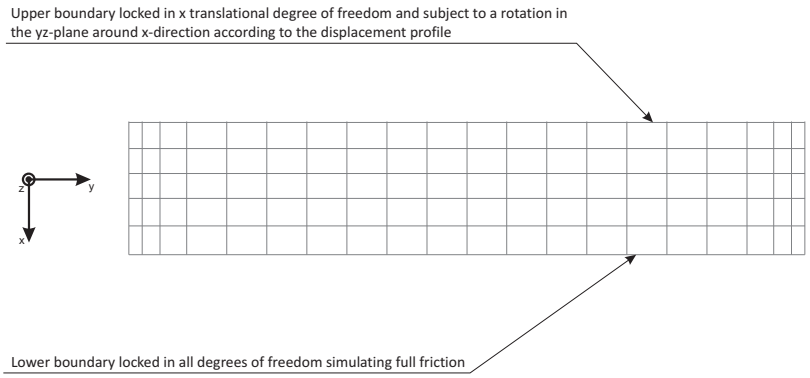

Figure 4.12: Hexa hedral mesh for simulation of rotational rheometer test, 200 hexahedrons

In figure 4.12 the mesh with a mesh density of 200 hexahedrons is shown used for the simulation of evaluation 2 experiment [15]. The mesh density has been established through a convergence study in appendix B and this mesh density is assumed for all three levels of strain rate. The friction has been assumed to be very high so as no slip occurs between the platens and the specimen, this allows the model to be constructed without contact formulation. Further the compressive force present during the torsion of the specimen has been assumed small enough to be neglected. It has been approximated to 20 Pa which is order of magnitude lower than the shear stresses.

4.3 Simulations

Experiment	Id	Material model	ν	C_1	C_2	μ_1	α_1	K	S_1	T_1	G_1	β_1	ρ	G_0
Calibration														
0.2/s	CIH5O1	Ogden Rubber	0.499	-	-	30	20	-	-	-	3000	310	920	-
	CIH5Si1	Simp. Rubber	0.49	-	-	-	-	5E5	-	-	-	-	920	-
	CIH5So1	Soft Tissue	-	100	100	-	-	5E5	10	0.00322	-	-	920	-
Calibration														
100/s	CJH2O1	Ogden Rubber	0.4999983	-	-	30	20	-	-	-	3000	310	920	-
	CJH8Si1	Simp. Rubber	0.49	-	-	-	-	5E8	-	-	-	-	920	-
	CJH2So1	Soft Tissue	-	100	100	-	-	5E8	10	0.00322	-	-	920	-
Evaluation 1														
	E1OH2O1	Ogden Rubber	0.499	-	-	30	20	-	-	-	3000	310	920	-
	E1OH2So1	Soft Tissue	-	100	100	-	-	5E5	10	0.00322	-	-	920	-
Evaluation 2														
1/s	E2TH2O1	Ogden Rubber	0.499	-	-	30	20	-	-	-	3000	310	920	-
	E2TH2So1	Soft Tissue	-	100	100	-	-	5E5	10	0.00322	-	-	920	-
	E2TH2T1	Viscoelastic	-	-	-	-	-	2.296E6	1.169E5	100	-	-	1200	3.506E5
Evaluation 2														
0.1/s	E2UH2O1	Ogden Rubber	0.499	-	-	30	20	-	-	-	3000	310	920	-
	E2UH2So1	Soft Tissue	-	100	100	-	-	5E5	10	0.00322	-	-	920	-
	E2UH2T1	Viscoelastic	-	100	100	-	-	2.296E6	1.169E5	100	-	-	1200	3.506E5
Evaluation 2														
0.01/s	E2VH2O1	Ogden Rubber	0.499	-	-	30	20	-	-	-	3000	310	920	-
	E2VH2So1	Soft Tissue	-	100	100	-	-	5E5	10	0.00322	-	-	920	-
	E2VH2T1	Viscoelastic	-	100	100	-	-	2.296E6	1.169E5	100	-	-	1200	3.506E5

Table 4.2: Table of material model parameters for simulations presented in the results section

In table 5.1 the simulations presented in the results section is shown. A detailed table of simulations is included in appendix G. Each simulation that is later presented in section 5 is described below. All other simulations are presented in their respective appendix.

4.3.1 Calibration

The parameter values used in the simulation of the calibration experiment [13] are the parameters obtained after some adjustments, hence the values are the final values. The parameters used for the Ogden Rubber model are μ_1, which is the shear modulus, α_1 which is hardening parameter, G_1 which is prony serie relaxation shear modulus and β_1 which is relaxation constant. Further a poisson's ratio of $\nu = 0.499$ is used for the low strain rate range and an implicit calculation is performed. For the intermediate strain rate range a poisson's ratio of $\nu = 0.4999983$ is used which corresponds, in small strain theory, to a bulk modulus of 0.5 GPa. The density used is $920kg/m^3$.

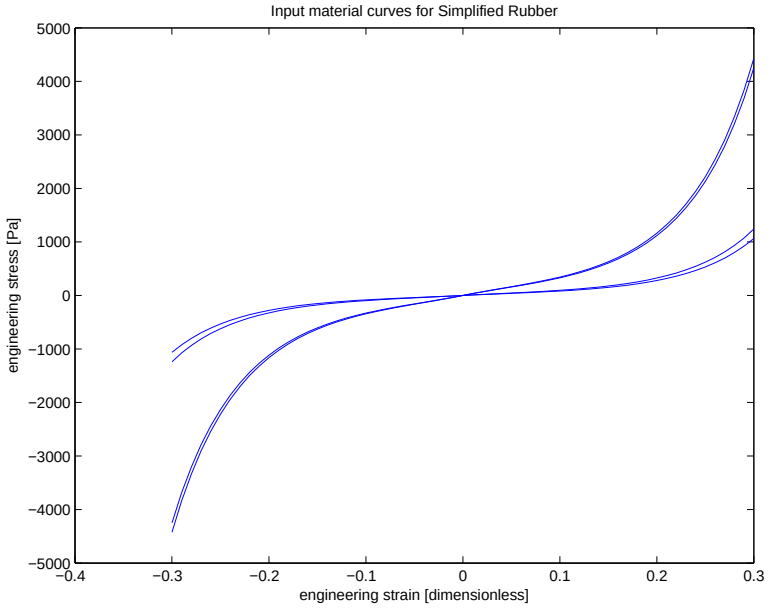

Figure 4.13: Input material curves for Simplified Rubber

For the Simplified Rubber model a bulk modulus of K=5E5 has been used for the low strain rate range and K=5E8 for the intermediate strain rate range. The material input curves are presented in figure 4.13. The curves are not taken directly from the experiment in [13] but are created by using an expression for the uniaxial tension of the incompressible Ogden Rubber without viscoelastic contribution [23]. The reason for using two curves at each range, two curves lies close to each other, is since if the strain rate is higher or lower than the one specified, the two curves closest to the actual rate will be used in the linear interpolation. The density is set to $920kg/m^3$.

When calibrating the Soft Tissue model the parameters C_1 and C_2 are varied which are stiffness parameters. Further the prony serie is input by varying the coefficients S_1 and T_1 which are the relaxation modulus and relaxation time respectively. The bulk modulus is set to K=5E5 for the low strain rate range and K=5E8 for the high strain rate range. The density is set to $920kg/m^3$.

4.3.2 Evaluation 1

These simulations are performed for the Ogden Rubber material model and the Soft Tissue material model only. The Simplified Rubber material model is discarded due to convergence problems. The parameters calibrated in the previous section are used, shown in table 5.1.

4.3.3 Evaluation 2

These simulations are performed for the Ogden Rubber material model and the Soft Tissue material model only. The Simplified Rubber material model is discarded due to convergence problems. The parameters calibrated in the previous section are evaluated. Also the THUMS model, Viscoelastic 006 in LS-DYNA [21] is simulated for reference. The parameters used are for the chest area of the THUMS HBM.

5 Results

The results section is divided into results from calibration [13], results from evaluation 1 [8] and evaluation 2 [15].

5.1 Results from calibration

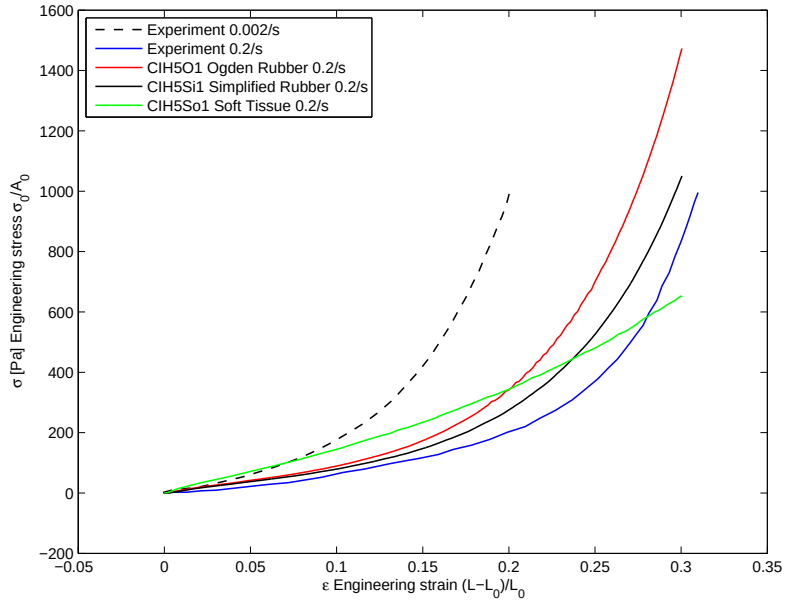

Figure 5.1: Experimental curves taken from [13]

Material model	ν	C_1	C_2	μ_1	α_1	K	S_1	T_1	G_1	β_1	ρ
Ogden Rubber	0.499	-	-	30	20	-	-	-	3000	310	920
Simp. Rubber	0.49	-	-	-	-	5E5	-	-	-	-	920
Soft Tissue	-	100	100	-	-	5E5	10	0.00322	-	-	920

Table 5.1: Table of material model parameters for low strain rate range

The experimental curves in figure 5.1 are taken from [13], from the low strain rate compression test. The experimental curves are chosen with 0.2/s and 0.002/s strain rate. These strain rates are the lowest and highest strain rates in the low strain rate region. The analyses are performed at a strain rate of 0.2/s. Note that the soft tissue material model is less nonlinear than the ogden model and the simplified rubber model.

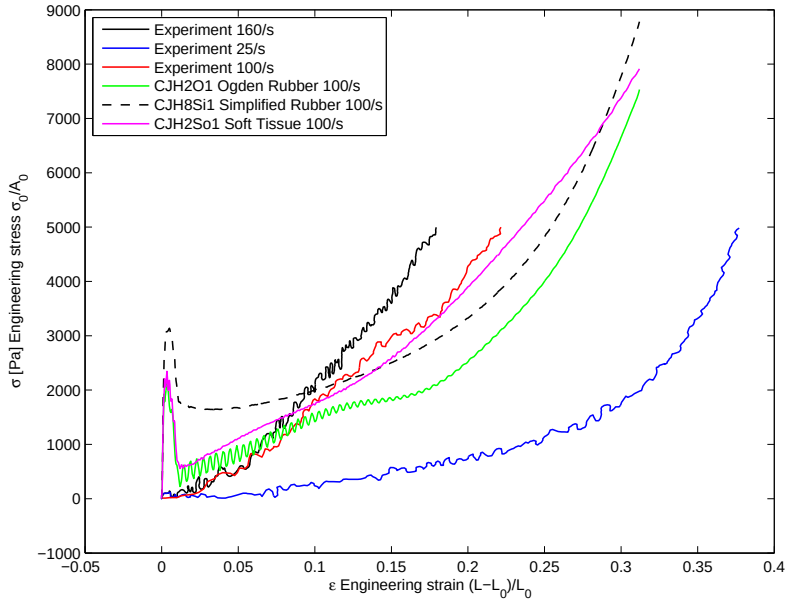

Figure 5.2: Experimental curves taken from [13]

The experimental curves in figure 5.2 are taken from [13], from the intermediate strain rate compression test. The experimental curves are chosen with 100/s and 160/s strain rate. Note that the curve from the simplified rubber model is higher than the curves from the other models. Also note the peak in the beginning of the curves from the analyses and note the abscence of this peak in the experiments.

Material model	ν	C_1	C_2	μ_1	α_1	K	S_1	T_1	G_1	β_1	ρ
Ogden Rubber	0.4999983	-	-	30	20	-	-	-	3000	310	920
Simp. Rubber	0.49	-	-	-	-	5E8	-	-	-	-	920
Soft Tissue	-	100	100	-	-	5E8	10	0.00322	-	-	920

Table 5.2: Table of material model parameters for intermediate strain rate range

5.2 Results from evaluation 1

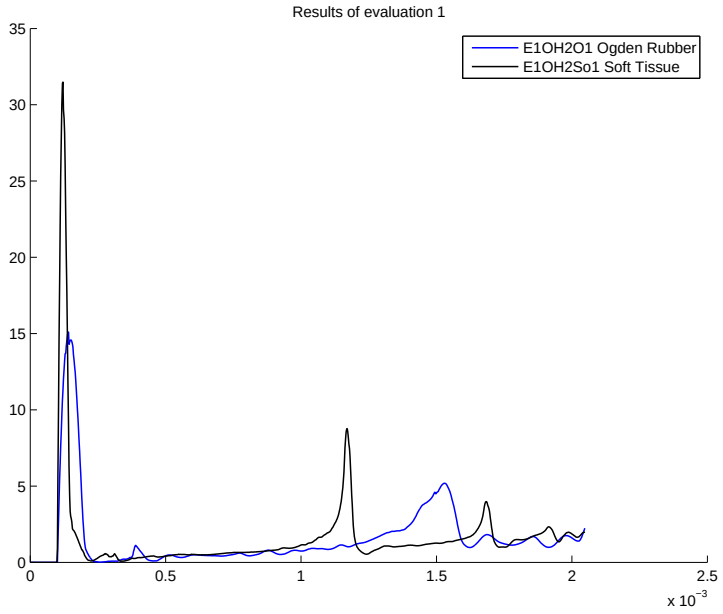

Figure 5.3: Ogden Rubber and Soft Tissue. Experimental curves taken from [8]

In figure 5.3 the results of evaluation 1 are presented. The Ogden Rubber and the Soft Tissue model are presented. Note that the end values are around 2 N which is 25 percent of the experimental reported force at 4 mm penetration. The parameters in table 5.2.

5.3 Results from evaluation 2

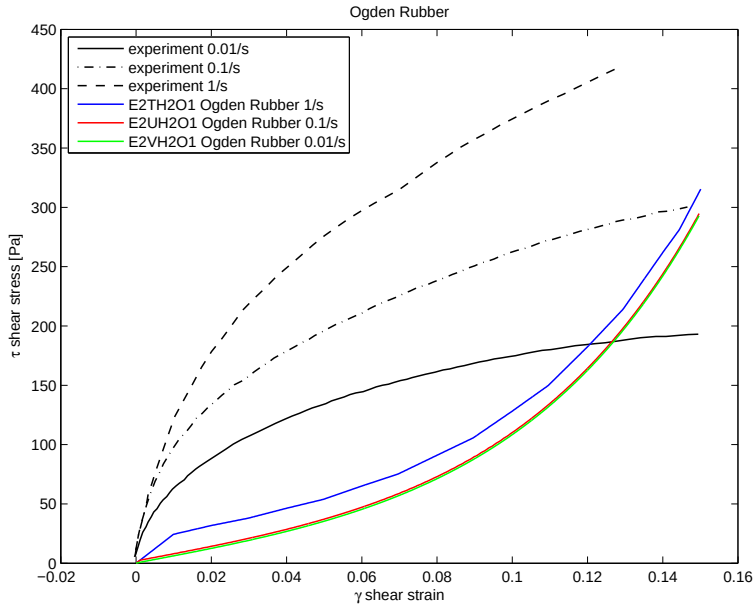

Figure 5.4: Ogden Rubber with linear viscoelasticity. Experimental curves taken from [15]

In figure 5.4 the ogden rubber model is compared to three different shear strain rates. Note the difference in the slope. The experiment shows shear strain softening and the simulation shows shear strain hardening.

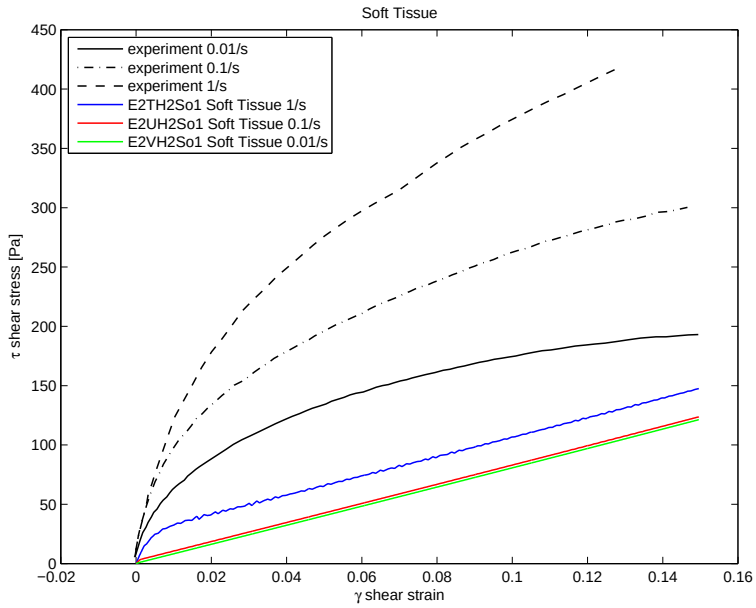

Figure 5.5: Soft Tissue with viscoelasticity. Experimental curves taken from [15]

In figure 5.5 the Soft Tissue model with viscoelasticity is simulated at three different shear strain rates. Note the almost linear behaviour of the Soft Tissue model and the shear strain softening of the experiment.

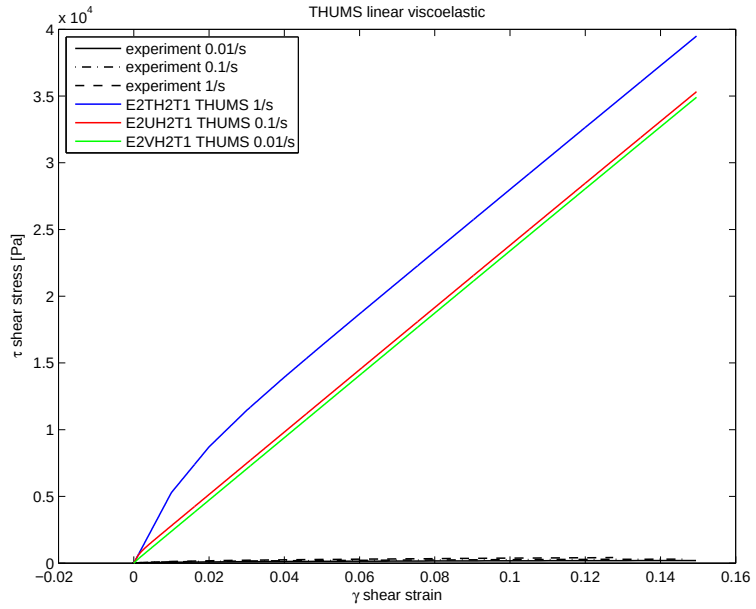

Figure 5.6: Viscoelastic material model. Experimental curves, at bottom of figure, taken from [15]

In figure 5.6 the THUMS material model is simulated at three different strain rates. Note the excess stiffness of the THUMS simulation. The experiments lies at the bottom of the graph.

The parameters in table 5.1 are used for Ogden Rubber and Soft Tissue. The THUMS material model parameters are ρ =1200 K=2.296E6 G_0=3.506E5 G_i=1.169E5 β=100 . The Simplified Rubber input curves are from figure 4.13.

6 Discussion

The discussion section will begin with an analysis of the results of the simulation of the calibration experiment. Proceeding with an analysis of the evaluation 1 experiment. Finally, a discussion of the result in the simulation of the experiment in evaluation 2.

6.1 Calibration

The Ogden rubber material model in figure 5.2 predicts the stress-strain behaviour in compression with excellent results. There is no need to make any improvements for the low strain rate region since the model is as good as the indata. The same applies to the Simplified Rubber material model 5.2. The soft tissue material model shows a weak nonlinear behaviour. This is due to when the parameters of the model are tweaked according to section 3.0.1 the model reduces to a Mooney Rivlin solid which is a special case of the two term Ogden Rubber with parameters $\alpha_1 = 2$ and $\alpha_2 = -2$. Since the Ogden Rubber model in figure 5.2 has parameter $\alpha = 20$ it is more nonlinear than the Mooney Rivlin which is of second order. The discrepancies between the Ogden Rubber model and the Simplified Rubber model is just a matter of parameter tweaking, they have equal behaviour.

When predicting the intermediate strain rate region a value of 100/s was choosen. It can be seen here also that the Soft Tissue model is less linear than the Ogden Rubber model, this difference is explained as previously. The peak in the beginning of the analysis comes from the inertial effects. Since the material is very compliant and the density rather high a small amount of acceleration gives a relatively large contribution to the overall forces. In the experiment there is no peak at the beginning. One possible explanation could be that the density is set too high but this is rather unlikely since the same value has been observed in different papers. A more possible explanation or hint to where an explanation could be found is in the test setup. It was not possible to obtain the blueprints of the loadcell and there might be something in its construction that filters these peaks.In the experiment the platen was accelerated upto the choosen velocity and then impacted onto the specimen. It was not possible to model this high acceleration, as in the impact, with this high bulk modulus without getting an unstable solution. With a higher acceleration the peak would become higher and thinner and could possibly be filtered away by the real test setup, it might not even be registered by the measuring device. Since all three material models has a peak in the beginning of the analysis it is less probable that the reason lies in the material modelling. The Soft Tissue is more similar to the Ogden rubber at this strain rate due to the fact that both has a viscoelastic contribution with a one term Prony serie as relaxation function. The Simplified Rubber model deviates from the other two models since it has no hereditary integral that constitutes a fading memory effect of the strain rate at previous timesteps. The Simplified Rubber has its stress-strain curve above the other material models and it is not possible to lower it any further at this strain rate and density. If the stiffness is reduced it asymptotically approaches a curve with the same peak as with the original stiffness and the remaining curve is less nonlinear.

6.2 Evaluation 1

According to figure 5.3 and table 4.1 the simulation results for both material models are only 25 percent of the experimental value in cycle 8. This could be due to several factors. For instance the indentor used in the experiment is flat ended and no radius is reported. Obviously it has to have a radius but how small it is is not documented. There hasn't been enough time in the project to make a study on the sensitivity of the force to the radius and a radius of 1 mm have been used. It could be speculated at least that the force should increase with decreasing radius but with what amount. The sensitivity might decrease with decreasing radius but that is just a speculation. In order to decrease numerical instability the indentor does not impact the specimen at full velocity rather accelerates from zero upto 2000 mm/s in 0.1 ms. This is only 5 percent of the total simulation time. Due to the relaxation time of 3.22 ms of the one term prony serie in both models this means that it does not have time to fully relax. If a longer relaxation time had been set it could be speculated that the force would be higher at 4mm penetration. Since the simulation time, due to the acceleration in the beginning, is a little bit longer than in reality the end value of the simulation will be lower since the viscoelastic contribution would have relaxed to a lower stiffness. This would result in a lower value of indentor force. It is quite riskful to compare one value since there are oscillations in the force and they could be shifted slightly in time due to different factors which would result in a value far away from the real value even though, if the whole experimental curve could have been obtained, it might have been really close in comparison. The opposite is also a risk. Further the ovine WAT might be stiffer than porcine or human WAT. In the experiment hexahedral elements were used with a 1 point integration solid element. Since they are subject to hourglassing, and hourglass formulation has been used. Unfortunately the hourglass forces are higher than the rule of thumb, below 10 percent of peak internal energy. An hourglass sensitivity study has been performed which reveals little sensitivity between indentor force and hourglass coefficient, see appendix D.1.2. This might support the use of higher than 10 percent hourglass energy.

6.3 Evaluation 2

According to figure 5.4 the Ogden Rubber predicts the stresses with reasonable accuracy but it exhibits an opposite behaviour considering the stiffness. This is due to the fact that the experiment shows shear strain softening and the model is calibrated against a compression curve with strain hardening. If the model is calibrated with compressive strain-hardening and tensile strain hardening it is unlikely that shear strain softening can fit in the model behaviour. Further the strain rate dependency is different in that the model does not show as large increase with strain rate as the experiment. This is due to the indata and can be accomodated by the model since more terms can be added to the prony series thus capturing a wider range of strain rates. In figure 5.4 looking at the curve of the Ogden rubber model at strain rate 1/s there is a small slope in the beginning with decreasing stiffness. This is from the hereditary integral with one prony serie fitted to the experiment in the calibration at 100/s. The small slope has similar behaviour as the experiment curves but if this small slope would be expanded by use of shorter relaxation times the compressive behaviour would also be influenced since the same prony serie is used for all elements of the strain rate tensor, that is the same prony serie is used for all shear strains and strains in the hereditary integral according to section 3.0.3.

In figure 5.4 it can be seen that the Simplified Rubber model has a similar behaviour as the Ogden Rubber in figure 5.4. The difference is that there is no slope in the beginning of the curve at strain rate 1/s since there is no heriditary integrals involved, only linear interpolation. This model cannot accomodate both tensile and compressive strain harden-

ing at the same time as shear strain softening since the input is a curve from a uniaxial tensile-compressive test. If shear strain softening is wished for the compressive and tensile strain hardening would suffer. The strain rate dependency for this model is constant at these ranges of strain due to the indata but the model can accomodate the strain rate stiffening response if the appropriate indata is input.

In figure 5.5 the results from the Soft Tissue material model is shown. This model is more similar in its shear stress-strain response than the previous models but this model cannot predict shear strain softening since it is linear in shear strain. The shear stress depends on the Mooney Rivlin coefficients added and then multiplied by the shear strain, that is the two Mooney Rivlin coefficients added is equal to the shear modulus. The model with these particular parameters is does not represent the same amount of shear strain stiffening but it can be accomodated if fitted with indata from the correct strain rate range. The slope at the beginning of the curve at strain rate 1/s has the same explanation as for the Ogden Rubber model in figure 5.4

Figure 5.6 displays the THUMS model which is the LS-DYNA linear viscoelastic model with one term prony serie. The experiment curves have been flattened out and lies at the bottom of the figure since this model severely overestimates the stiffness and shear stress by a factor 10^2.

7 Conclusions

The Ogden Rubber would be suitable if range of strain rate is not too large otherwise the Soft Tissue is a better choice while the Simplified Rubber is discarded due to severe convergence problems. The Ogden Rubber would be the preferred choice if a strongly nonlinear behaviour in compressive-strain to compressive-stress is sought for. The Soft Tissue would be more suitable if there are large shear strains that affect the human body model. The Ogden Rubber would be preferred if incorrect shear strain representation and narrow range of strain rate is weighed up by it being 6-7 times faster. Which model that is the most preferred would be determined by future work and investigations.

8 Future Work

It is highly recommended to do further experiments on WAT due to paucity of available experiments and due to the small number of specimens and samples used in the up to now conducted experiments. It is suggested tha porcine WAT be used since it is similar to human WAT. Especially, subcutaneous WAT at the porcine back middle layer which is similar to deep subcutaneous WAT at the human abdomen [14]. Further, investigations are needed on finding a similar depot site of the visceral human WAT, since this depot site is relatively large in certain individuals.

Suggested experimental methods are unconfined compression, see work by [13]. There haven't been conducted any experiments on the tensile behaviour of WAT, due to difficulties in fastening of the specimen.

For evaluation an indentation experiment might be suitable since it produces a complex strain field including all strain components such as, shear, compression and tension. For indentation experiments see work by [4]. If indentation is going to be used it is recommended not to use a flat ended cylindrical indentor but rather one that has a radius at the end. This is to get rid of the sharp edge which is troublesome when modeling contact since it complicates contact modeling by introducing a lot of hourglassing due to the concentraded stress at the edge. A sharp edge does also require a higher mesh density in order for the solution to converge, at least for convergence of the contact force.

Regarding the material models of this thesis, if one is going to be used it is recommended to investigate the need to correctly represent the shear strains in an actual crash simulation since both models underestimates the stiffness in shear for small values of strain and overestimates for higher values of strain. Further a sensitivity analysis should be performed for the wanted quantities with respect to the bulk modulus. This is since the bulk modulus of WAT is rather high which in turn slows down the explicit calculations considerably. If the Ogden Rubber model is to be used, a sensitivity study of the wanted quantities with respect to the poisson ratio is recommended since a very high poissons ratio, very close to 0.5, indirectly increases the bulk modulus which in turn slows down explicit calculations.

References

[1] Saverio Cinti. The role of brown adipose tissue in human obesity. *Nutrition, Metabolism & Cardiovascular Diseases*, 16:569–574, 2006.

[2] Kerstyn Comley. A micromechanical model for the young's modulus of adipose tissue. *International Journal of Solids and Structures*, 47:2982–2990, 2010.

[3] Livermore Software Technology Corporation. Ls-pre/post. `http://www.lstc.com/lspp`, August 2011.

[4] Abbas Samani et al. A method to measure the hyperelastic parameters of exvivo breast tissue samples. *Phys Med Biol*, 49:4395–4405, 2004.

[5] Abbas Samani et al. Elastic moduli of normal and pathological human breast tissues an inversion-technique-based investigation of 169 samples. *Phys Med Biol*, 52:1565–1576, 2007.

[6] Alison Sharpe Avram et al. Subcutaneous fat in normal and diseased states: 2. anatomy and physiology of white and brown adipose tissue. *Journal of the American Academy of Dermatology*, 53:671–683, 2005.

[7] A.M. Sims et al. Elastic and viscoelastic properties of porcine subdermal fat using mri and inverse fea. *Biomech Model Mechanobiol*, 9:703–711, 2010.

[8] Amit Gefen et al. Viscoelastic properties of ovine adipose tissue covering the gluteus muscles. *Journal of Biomedical Engineering*, 129:924–930, 2007.

[9] Dietrich Jehle MD et al. Influence of obesity on mortality of drivers in severe motor vehicle crashes. *The american journal of emergency medicine*, 234:34, 2010.

[10] D.J. Benson et al. A simplified approach for strain-rate dependent hyperelastic materials with damage. Technical report, University of Californa, Dept. of Mechanical and Aerospace Engineering, San Diego, USA; Daimler Chrysler AG, Sindelfingen, Germany; Consulting Engineer, Offenbach, Germany, 2006.

[11] Geerligs et al. Linear viscoelastic behaviour of subcutaneous adipose tissue. *Biorheology*, 45:677–688, 2008.

[12] Javier Bonet et al. *Nonlinear continuum mechanics for finite element analysis*. Cambridge University Press, 2008.

[13] Kerstyn Comley et al. The mechanical response of porcine adipose tissue. *ASME Journal of Biomechanical Engineering*, 2009.

[14] Klein et al. What are subcutaneous adipocytes really good for, viewpoint 5. *Experimental Dermatology*, 16:45–70, 2007.

[15] Marion Geerligs et al. Does subcutaneous adipose tissue behave asan(anti-)thixotropic material? *Journal of Biomechanics*, 43:1153–1159, 2010.

[16] Martin AD et al. Adipose tissue density, estimated adipose lipid fraction and whole body adiposity in male cadavers. *International Journal of Obesity Related Metabolic Disorders*, 18(2):79–83, 1994.

[17] Maurovich-Horvat et al. Comparison of anthropometric, area- and volumebased assessment of abdominal subcutaneous and visceral adipose tissue volumes using multidetector computed tomography. *International Journal of Obesity*, 31:500–506, 2007.

[18] Noriyuki Ouchi et al. Adipokines in inflammation and metabolic disease. *Nature Reviews Immunology*, 11:85–97, 2011.

[19] Parul Natvar Patel et al. Rheological and recovery properties of poly(ethyleneglycol) diacrylate hydrogels and human adipose tissue. Technical report, Department of Chemical Engineering, Rice University, Houston, Texas 77005 Laboratory of Reparative Biology and Bioengineering, Department of Plastic Surgery, The University of Texas M.D., 2004.

[20] John O. Hallquist. *LS-DYNA theory manual*. LSTC, 2006.

[21] LSTC. *LS-DYNA Keyword User's Manual*. LSTC, 2010.

[22] Kenneth Runesson. *Constitutive Modeling of Engineering Materials - Theory and Computation*. Chalmers University of Technology, 2006.

[23] Wikipedia. Ogden (hyperelastic model). `http://en.wikipedia.org/wiki/Ogden_(hyperelastic_model)`, Junet 2011.

[24] ZENBIO. Visceral preadipocytes and adipocytes. *ZENBIO*, 1:1, 2009.

A Finite Deformation Continuum Mechanics

A.1 Finite Deformation Kinematics

The motion of a body can be described by the mapping

$$\mathbf{x} = \Phi(\mathbf{X}, t) \tag{A.1}$$

This mapping is a transformation from the Lagrangian, material, formulation to the Eularian, spatial, formulation. It is a transformation from the undeformed to the deformed configuration. In order to transform quantities between the material and spatial configuration the deformation gradient is defined

$$\mathbf{F} = \frac{\partial \Phi(\mathbf{X}, t)}{\partial \mathbf{X}} \tag{A.2}$$

In order to get a representation of the strain the right Cauchy-Green deformation tensor is defined as

$$\mathbf{C} = \mathbf{F}^{\mathbf{T}}\mathbf{F} \tag{A.3}$$

This can be interpreted as the transformation of the scalar product between two elemental vectors in the material configuration to the spatial configuration

$$d\mathbf{x}_1 \cdot d\mathbf{x}_2 = d\mathbf{X}_1 \cdot \mathbf{C} d\mathbf{X}_2 \tag{A.4}$$

In order to calculate the difference between the scalar product of the elemental vectors above the Green strain tensor is introduced

$$\mathbf{E} = \frac{1}{2}(\mathbf{C} - \mathbf{I}) \tag{A.5}$$

This then becomes

$$\frac{1}{2}(d\mathbf{x}_1 \cdot d\mathbf{x}_2 - d\mathbf{X}_1 \cdot d\mathbf{X}_2) = d\mathbf{X}_1 \cdot \mathbf{E} d\mathbf{X}_2 \tag{A.6}$$

The Green strain tensor is the equivalent of the small strain tensor in infinitesimal strain theory since the infinitesimal strain tensor is obtained upon linearization of the Green strain tensor

In order to pave the way for the viscoelastic contribution further on an expression for the velocity is needed.

$$\mathbf{v}(\mathbf{X}, t) = \frac{\partial \phi(\mathbf{X}, \mathbf{t})}{\partial t} \tag{A.7}$$

The above expression is differentiated with respect to the coordinates of the particles in the body in the material configuration which produces the time derivative of the deformation gradient

$$\dot{\mathbf{F}} = \frac{\partial}{\partial \mathbf{X}}(\frac{\partial \phi}{\partial t}) \tag{A.8}$$

The material time derivative of the Green strain tensor is also needed.

$$\dot{\mathbf{E}} = \frac{1}{2}(\dot{\mathbf{F}^{\mathbf{T}}}\mathbf{F} + \mathbf{F}^{\mathbf{T}}\dot{\mathbf{F}}) \tag{A.9}$$

To show how the above quantities are explicitly calculated an example of pure elongation will be used

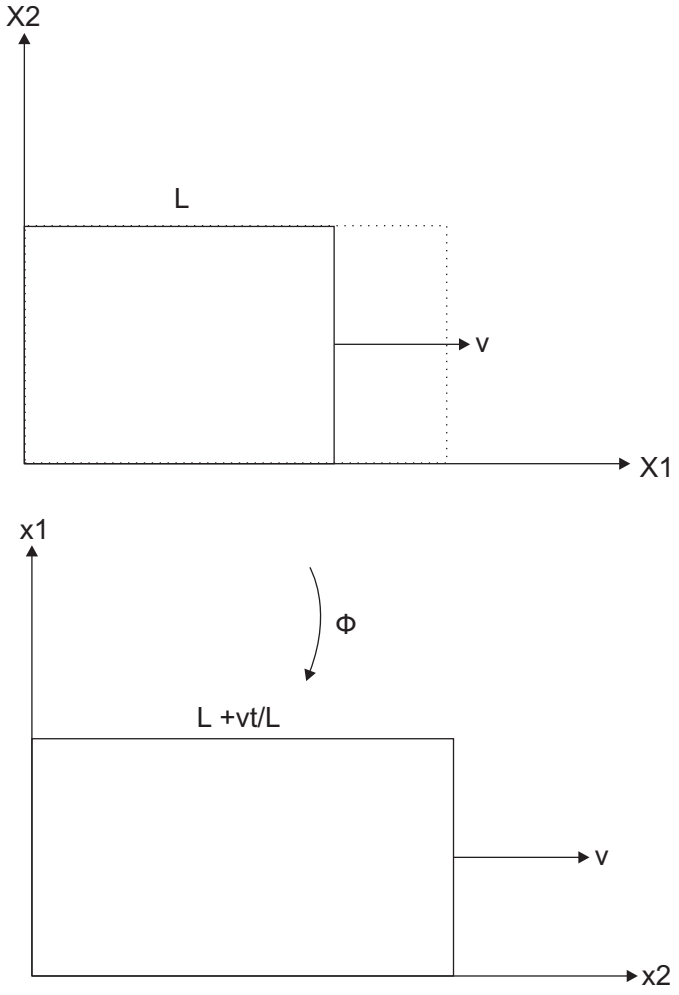

Figure A.1: Pure elongation

The displacement is the same as the above mentioned mapping

$$\mathbf{x} = \phi(\mathbf{X}, t) \tag{A.10}$$

The components of the displacement vector in this case becomes

$$x_1 = X_1 + X_1 vt/L \tag{A.11}$$
$$x_2 = X_2 \tag{A.12}$$
$$x_3 = X_3 \tag{A.13}$$

where v is the velocity of the right edge in the material configuration, t is time and L is the initial length.

$$\mathbf{F} = \frac{\partial \mathbf{x}}{\partial \mathbf{X}} = \begin{bmatrix} 1 + vt/L & 0 & 0 \\ 0 & 1 & 0 \\ 0 & 0 & 1 \end{bmatrix} \tag{A.14}$$

$$\dot{\mathbf{F}} = \frac{\partial}{\partial \mathbf{X}}\left(\frac{\partial \phi}{\partial t}\right) = \begin{bmatrix} v/L & 0 & 0 \\ 0 & 0 & 0 \\ 0 & 0 & 0 \end{bmatrix} \tag{A.15}$$

A.2 Stress Measures

The cauchy stress tensor is related to areas and forces in the current configuration, the deformed configuration, in the following way.

$$d\mathbf{p} = \sigma d\mathbf{a} \tag{A.16}$$

That is the common intuitive interpretation of stress. The second Piola-Kirchhoff stress tensor is instead a transformation of the cauchy stress into the initial configuration, the undeformed configuration. First, a pullback from the current to the initial configuration of the elemental force vector $d\mathbf{p}$ is performed.

$$d\mathcal{P} = \mathbf{F}^{-1} d\mathbf{p} \tag{A.17}$$

Now equation (A.16) is inserted into equation (A.17) resulting in

$$d\mathcal{P} = \mathbf{F}^{-1} \sigma d\mathbf{a} \tag{A.18}$$

The area elemental vector is still in the deformed configuration. Nanson's formula is used in order to transform it into the undeformed configuration

$$d\mathcal{P} = \underbrace{J\mathbf{F}^{-1}\sigma\mathbf{F}^{T}}_{\mathbf{S}} d\mathbf{A} \tag{A.19}$$

A.3 Hyperelasticity

Hyperelasticity is defined as path independency of the material. That is the strain energy function is only dependent on the initial and final state and not how that state was reached[12]. This can be formulated as

$$\Psi(\mathbf{C}(\mathbf{X}), \mathbf{X}) \tag{A.20}$$

$$\Psi(I_C, II_C, III_C, \mathbf{X}) \tag{A.21}$$

Ψ is the strain energy function. A definition of $\mathbf{C}$ can be found in appendix A.1. I_C, II_C, III_C are the first, second and third invariant of a second order tensor and are equal to $\mathbf{I} : \mathbf{C}$, $\mathbf{C} : \mathbf{C}$ and $det(\mathbf{C})$ respectively. In (A.21) the strain energy is dependent not upon C but only on its invariants which are invariant when the coordinate system is rotated. Since this is isotropic hyperelasticity the strain energy is fully determined by the three invariants. In for example transverse isotropy two additional invariants are needed in order to determine the strain energy. Below is the expression for the second Piola Kirchhoff stress tensor for an isotropic material.

$$\mathbf{S} = 2\frac{\partial \Psi}{\partial \mathbf{C}} = 2\frac{\partial \Psi}{\partial I_{\mathbf{C}}}\frac{\partial I_{\mathbf{C}}}{\partial \mathbf{C}} + 2\frac{\partial \Psi}{\partial II_{\mathbf{C}}}\frac{\partial II_{\mathbf{C}}}{\partial \mathbf{C}} + 2\frac{\partial \Psi}{\partial III_{\mathbf{C}}}\frac{\partial III_{\mathbf{C}}}{\partial \mathbf{C}} \tag{A.22}$$

A.4 Hyperelasticity in Principal Directions

When looking at an isotropic hyperelastic material in the principal directions the strain energy is a function of the principal stretches instead of the invariants of the right Cauchy Green strain tensor. In order to achieve this the square of the principal stretches and the

principal directions are obtained by calculating the eigenvalues and eigenvectors of C. This gives the expression for the second Piola Kirchhoff stress tensor as[12].

$$\mathbf{S} = \sum_{\alpha=1}^{3} S_{\alpha\alpha}\mathbf{N}_\alpha \otimes \mathbf{N}_\alpha; \mathbf{S}_{\alpha\alpha} = 2\frac{\partial \Psi}{\partial \lambda_\alpha^2} \tag{A.23}$$

The above equation is the spectral representation of the second Piola Kirchhoff stress tensor with the basevectors in the material configuration

A.5 Near incompressibility

When dealing with incompressible materials problems arise when used with the finite element method[12]. In order to get around this problem a nearly incompressible formulation is used instead where the strain energy is split into an isochoric and volumetric part as follows.

$$\Psi(\lambda_1, \lambda_2, \lambda_3) = \hat{\Psi}(\hat{\lambda_1}, \hat{\lambda_2}, \hat{\lambda_3}) + U(J) \tag{A.24}$$

The hat refers to isochoric deformation which is the deformation under constant volume. This implies that the determinant of the deformation gradient, the volume change, is equal to 1 and in the case of isotropy in principal directions this yields

$$\lambda_\alpha = J^{1/3}\hat{\lambda_\alpha} \tag{A.25}$$

The term U(J) is the energy generated when the body experience volumetric deformation and since near incompressiblity is used as an approximation for incompressibility, U(J) needs to be accompanied by a penalty parameter that forces the body not to deform volumetrically. That is it prohibits this way of deformation since due to the penalty parameter a volumetric deformation would give a considerable contribution to the strain energy as compared to isochoric deformation.

B Mesh Convergence

B.1 Calibration

In order to find out how many elements that are needed for the analyses a mesh convergence study is performed using successively larger mesh densities.

B.1.1 Hexahedral elements

The element used here is the default formulation in LS-DYNA, namely elform=1.

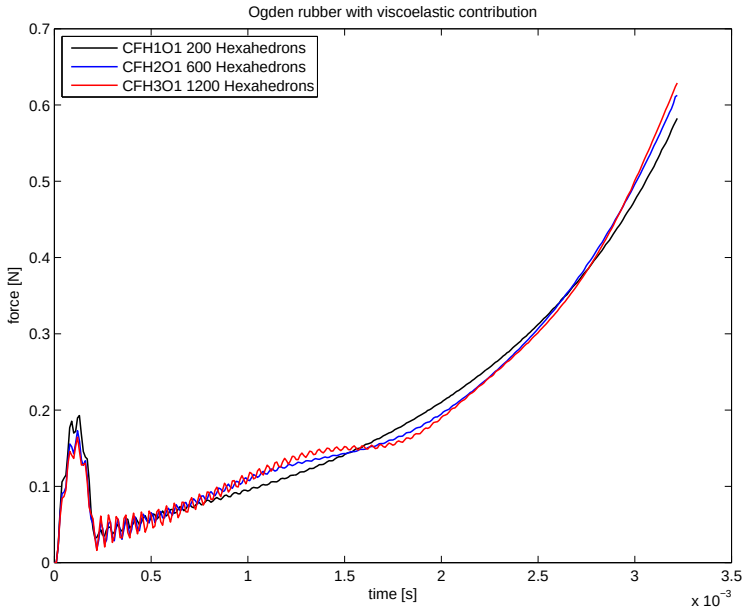

Figure B.1: Mesh convergence with explicit calculation. Ogden model with viscoelastic contribution

According to figure B.1 it can be concluded that for the ogden model with viscoelastic contribution it is sufficient with a mesh density with 600 hexahedrons for explicit calculations.

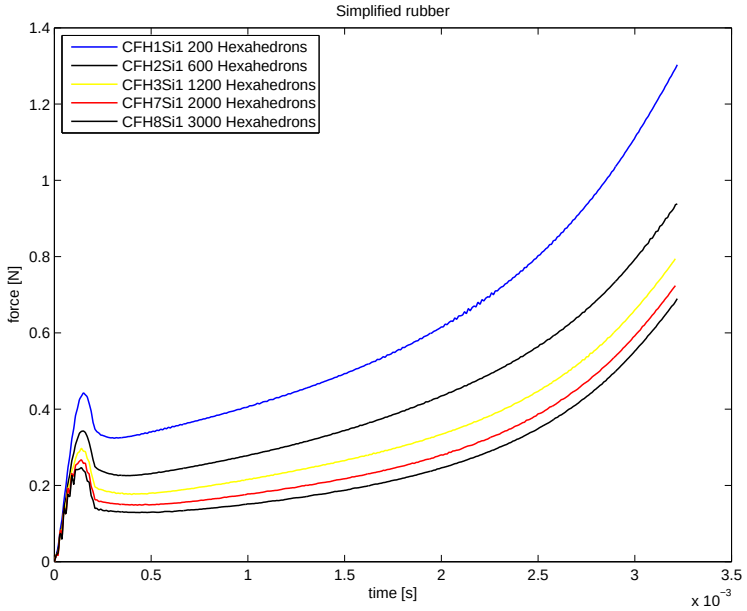

Figure B.2: Mesh convergence with explicit calculation.Simplified rubber with strain rate dependency

In figure B.2 it can be seen that the Simplified Rubber model requires around 2000 hexahedral elements in order to reach convergence. This is around 3 times more than the Ogden rubber model with viscoelastic contribution in figure B.1.

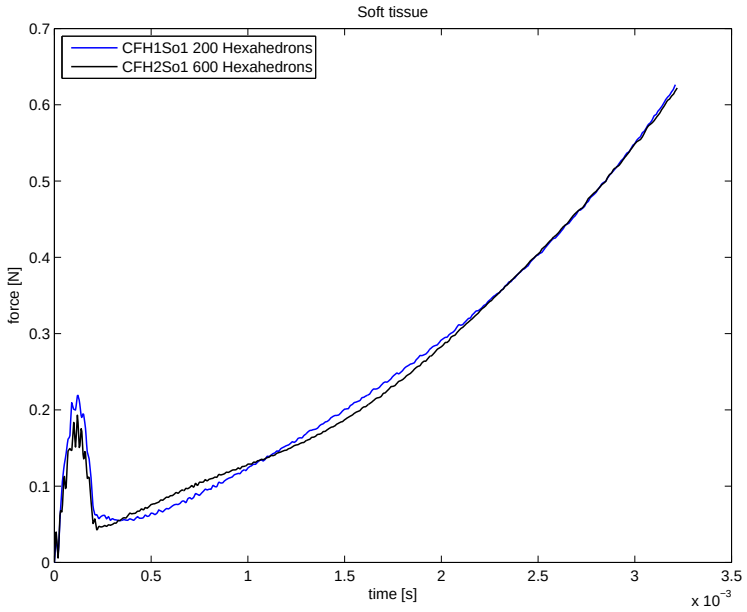

Figure B.3: Mesh convergence with explicit calculation. Soft tissue with viscoelastic contribution

In figure B.3 it can be seen that the Soft tissue model with viscoelastic contribution reaches convergence with 600 hexahedral elements.

B.1.2 Tetrahedral elements

The element used here is a tetrahedral formulation in LS-DYNA, namely elform=13.

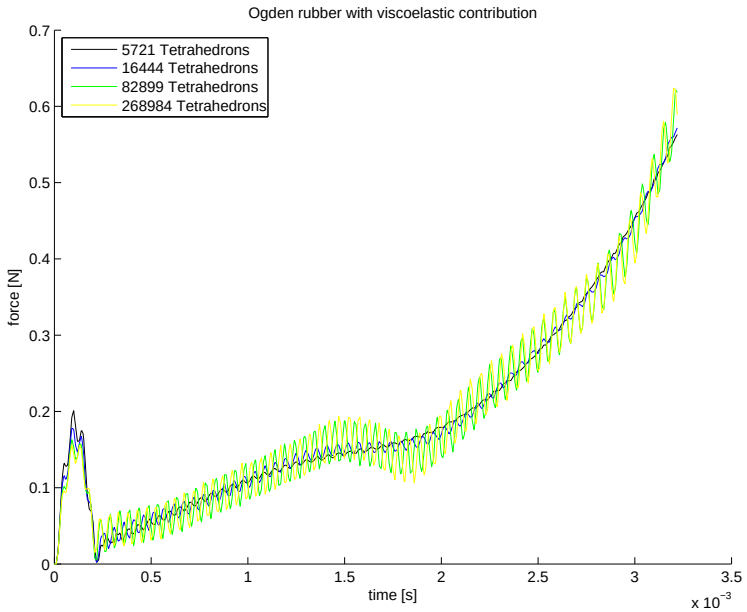

Figure B.4: Mesh convergence with explicit calculation. Ogden model with viscoelastic contribution

It can be seen in figure B.4 that there is sufficient convergence at 5721 tetrahedrons.

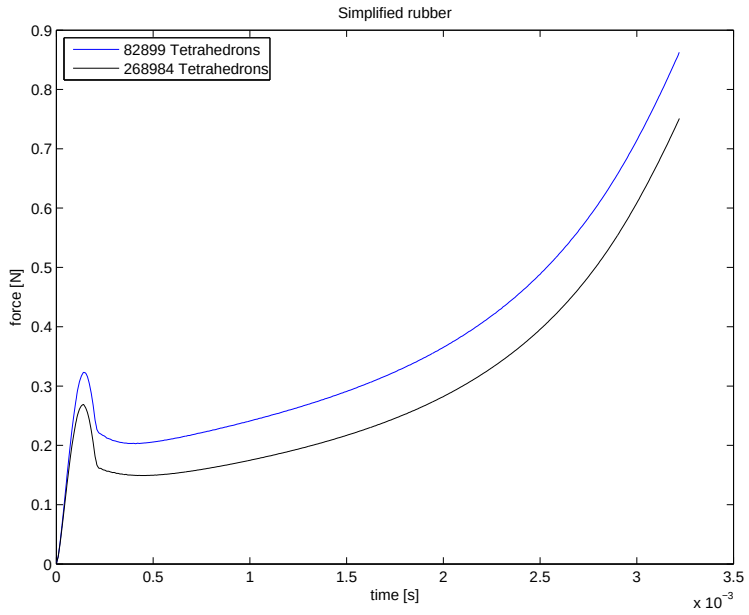

Figure B.5: Mesh convergence with explicit calculation. Simplified rubber with strain rate dependency

According to figure B.5 the Simplified rubber model does not converge even at 268984 tetrahedrons. No further increase in mesh density is necessary since the number of elements largely exceeds the number required for convergence of the Ogden rubber and Soft tissue model.

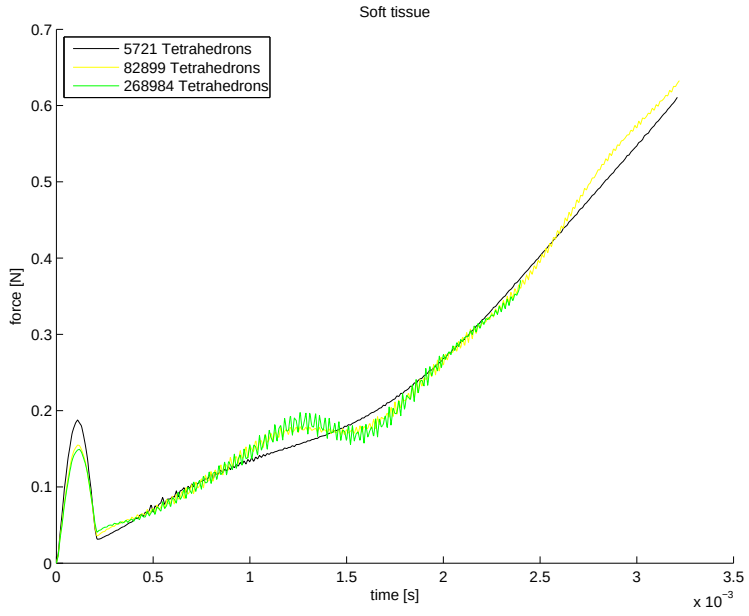

Figure B.6: Mesh convergence with explicit calculation.Soft tissue with viscoelastic contribution

It can be seen in figure B.6 that there is sufficient convergence at 5721 tetrahedrons.

B.2 Evaluation 1

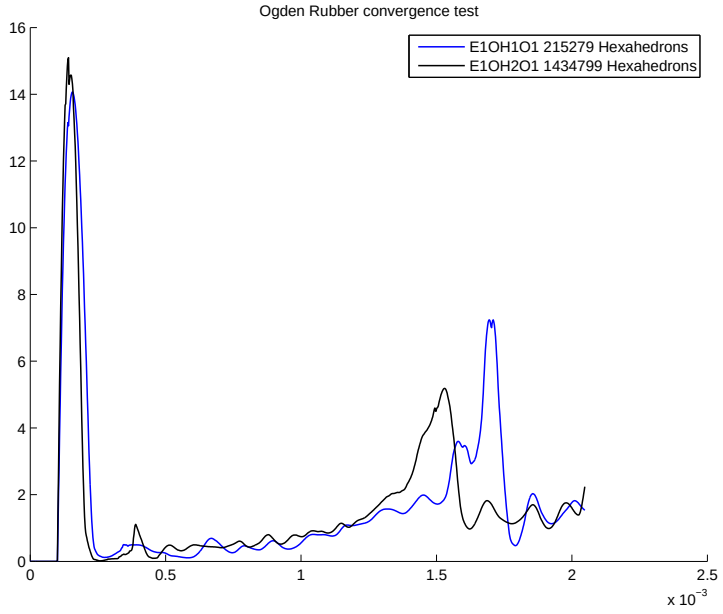

Figure B.7: Mesh convergence with explicit calculation. Ogden model with viscoelastic contribution

According to figure **??** it is reasonable to use a mesh density of 215279 hexahedrons for evaluation 2 with the Ogden Rubber material model.

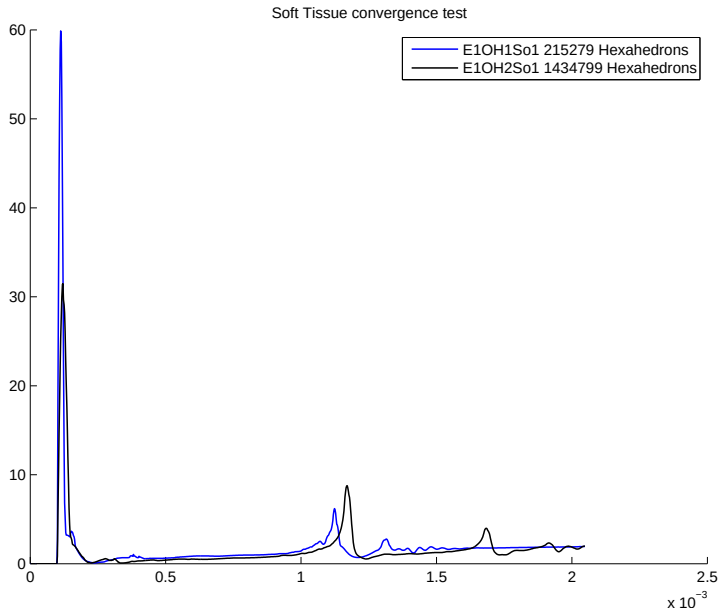

Figure B.8: Mesh convergence with explicit calculation. Soft Tissue with viscoelastic contribution

According to figure B.8 it is reasonable to use a mesh density of 215279 hexahedrons for evaluation 2 with the Soft Tissue material model.

B.3 Evaluation 2

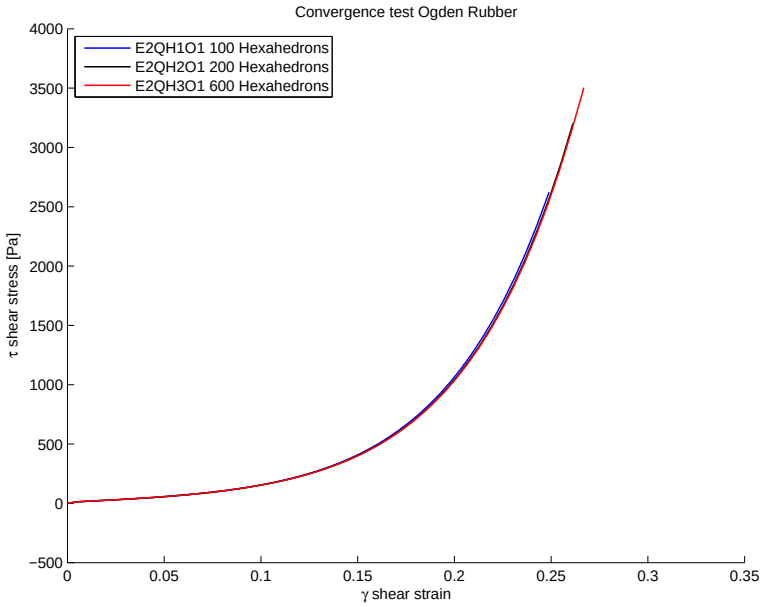

Figure B.9: Mesh convergence with implicit calculation. Ogden model with viscoelastic contribution

According to figure B.9 it can be concluded that for the ogden model with viscoelastic contribution it is sufficient with a mesh density with 200 hexahedrons for implicit calculations.

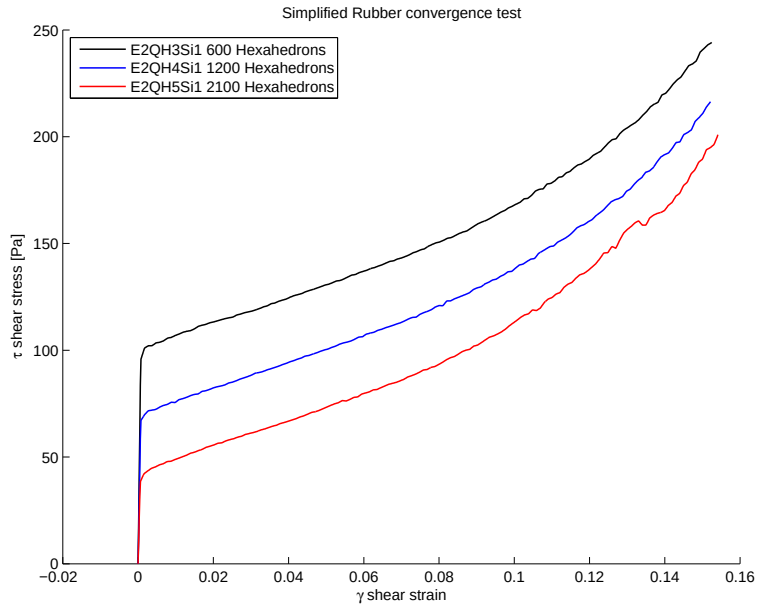

Figure B.10: Mesh convergence with explicit calculation.Simplified Rubber with strain rate dependency

It can be seen in figure B.10 that convergence is not reached even at 2100 hexahedrons. This model is therefore discarded since it demands at lowest a factor of ten times more than the Ogden Rubber to reach convergence.

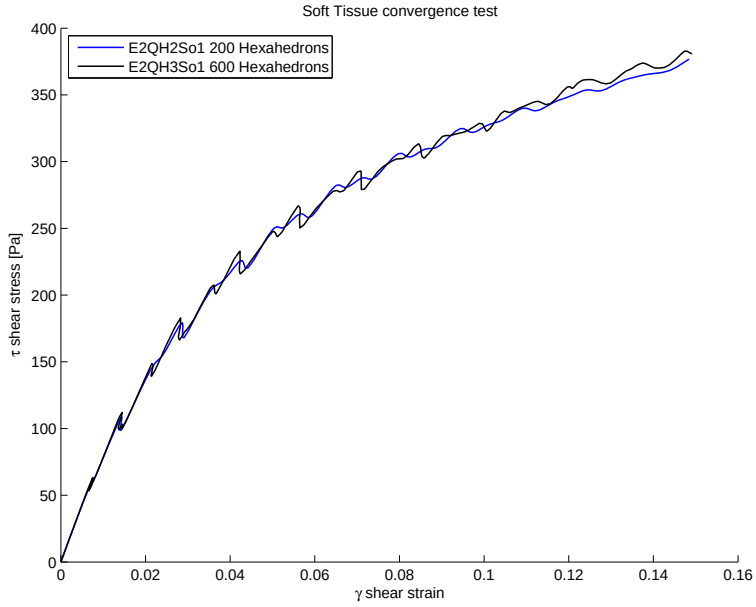

Figure B.11: Mesh convergence with explicit calculation.Soft Tissue with viscoelastic contribution

As can be seen in figure B.11 a mesh of 200 hexahedrons is sufficient for convergence.

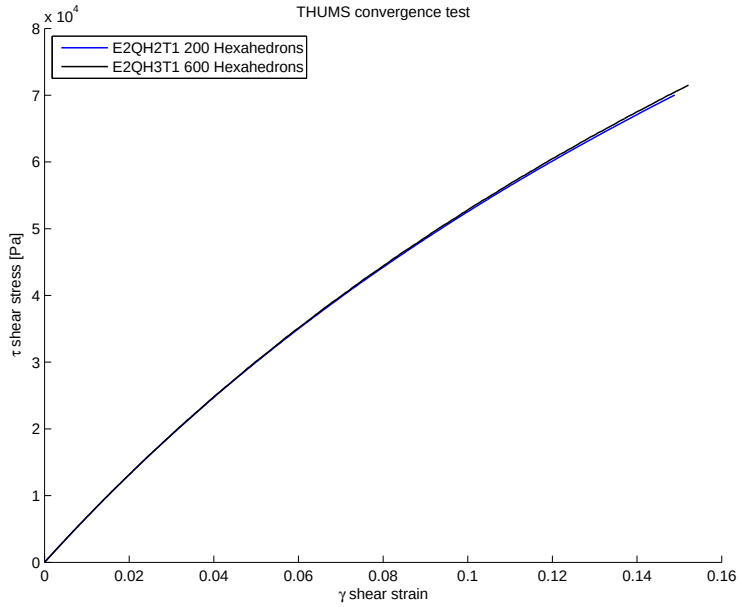

Figure B.12: Mesh convergence with explicit calculation.THUMS

According to figure B.12 it is considered safe to use a mesh density of 200 hexahedrons.

C Element formulation study

C.1 Element formulation Study

Since tetrahedral elements are going to be used in the future when meshing the WAT, an element formulation study has been performed comparing the converged hexahedral solution with different element densities of the tetrahedral formulation.

C.1.1 Calibration

The hydraulic compression test has been used and the converged

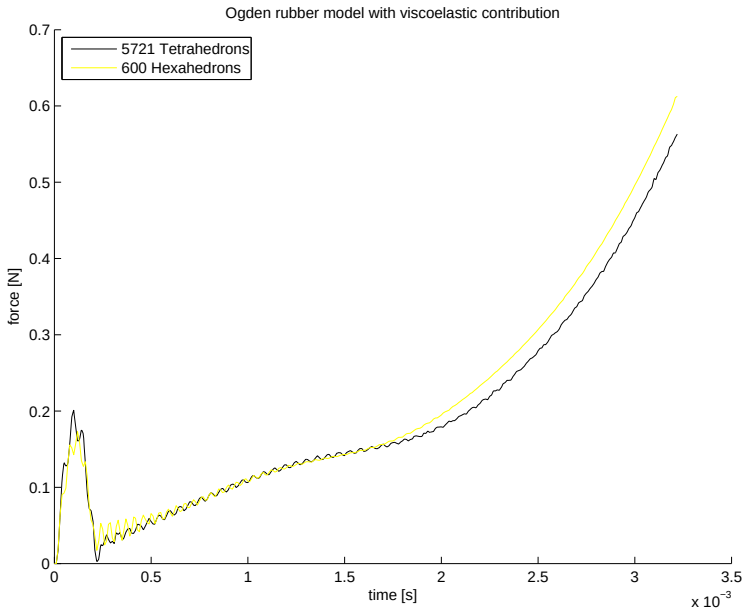

Figure C.1: Ogden rubber model with viscoelastic contribution.

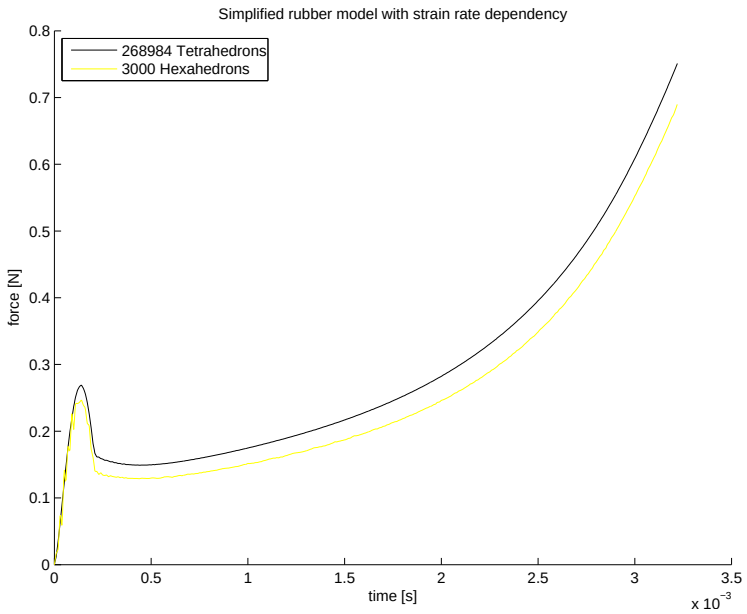

Figure C.2: Simplified model with strain rate dependency.

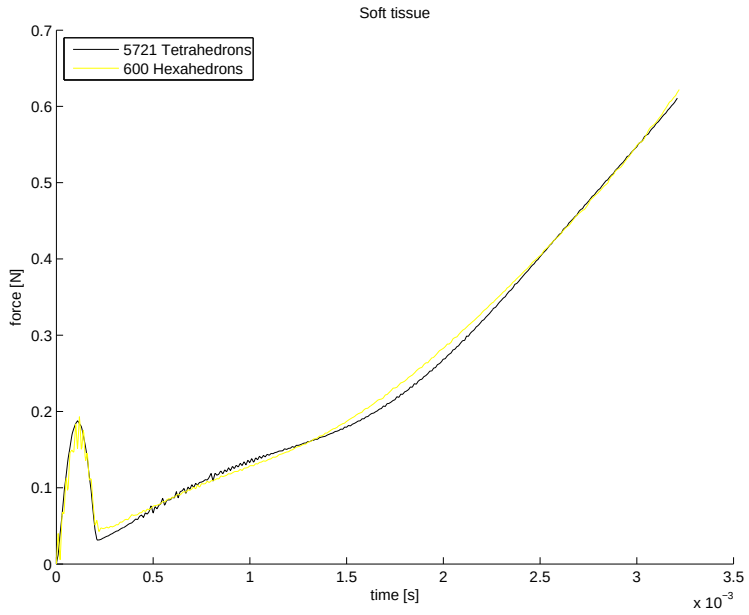

Figure C.3: Soft tissue model with viscoelastic contribution.

	seconds/Tetrahedron at 5721 elements	seconds/Tetrahedron at 268984 elements
Ogden rubber	0.01	0.04
Simplified rubber	0.03	0.13
Soft tissue	0.07	0.23

Table C.1: Element processing as if run with 1 CPU.

	speed factor
Ogden rubber - Simplified rubber	3
Simplified rubber - Soft tissue	2
Ogden rubber - Soft tissue	6-7

Table C.2: Table shows seconds/tetrahedron for the fastest material model, amongst the two compared, divided by seconds/tetrahedron for the slowest amongst the two compared.

The simulations has not been run with only one CPU hence their might be communication between the CPU:s in the element processing time, but the speed factors in table C.2 gives a hint of which ones the fastest, middle, and slowest.

D Hourglass formulation study

D.1 Hourglass formulation study

In order to find the appropriate hourglass formulation and hourglass coefficient a number of different formulations and coefficient have been tested at one strain rate with one material model.

D.1.1 Calibration

In these tests the Ogden model is used with $\mu = 40$, $\alpha = 20$ and a viscoelastic contribution by a one term prony serie with coefficients $\beta_1 = 310$ and $G_1 = 3000$. The engineering strain rate is 100/s.

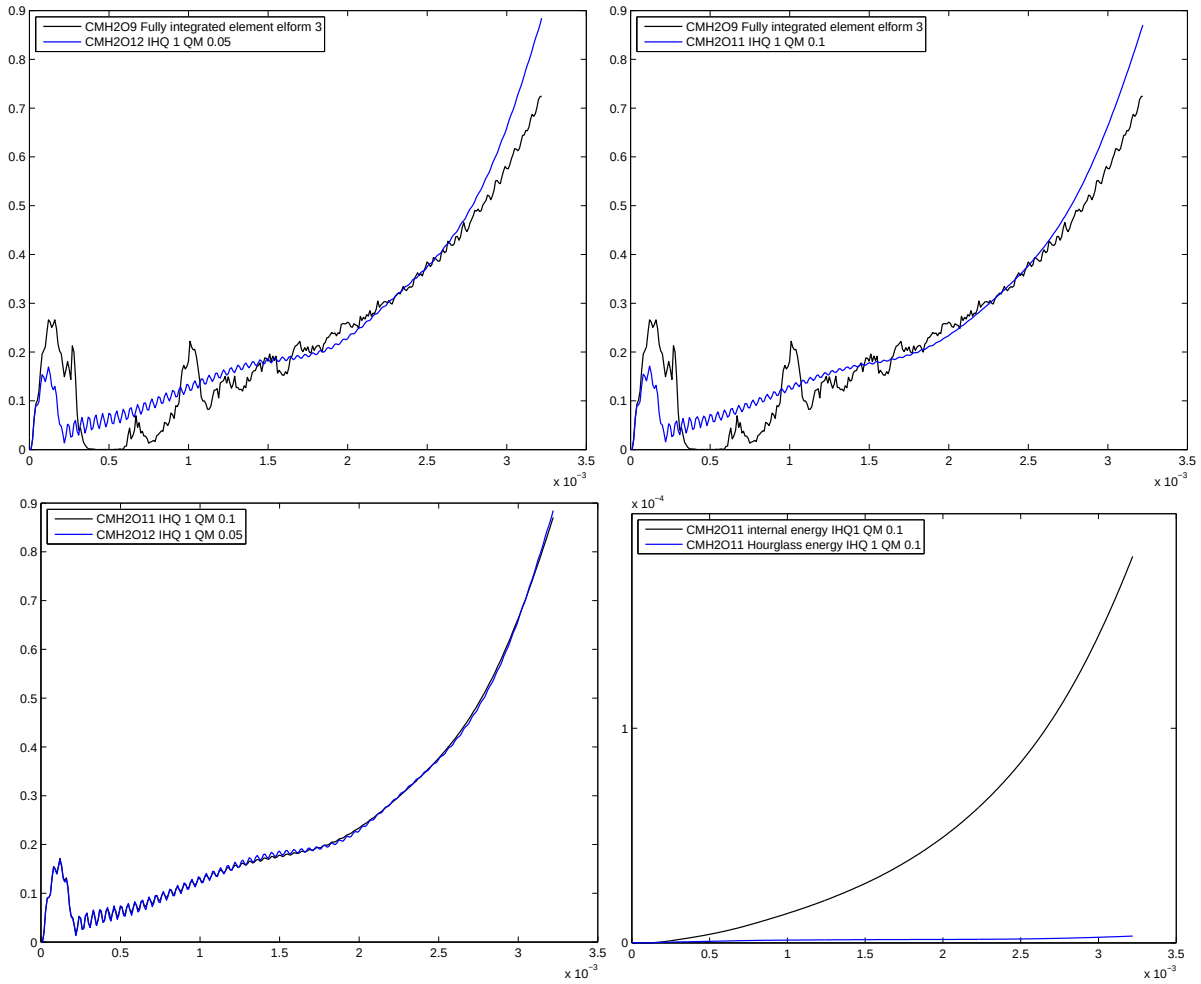

Figure D.1: Hourglass formulation study, mesh density 600 hexahedrons

According to figure D.1 a) it can be seen that the curve with 1 integration point element is sufficiently similar to the fully integrated element. Further according to figure D.1 c) there is almost no difference between an hourglasscoefficient of 0.1 and 0.05 since the curve almost overlaps. In figure D.1 d) it can be seen that the hourglass energy is very low in comparison with the internal energy and this formulation is used further on.

D.1.2 Evaluation Study 1

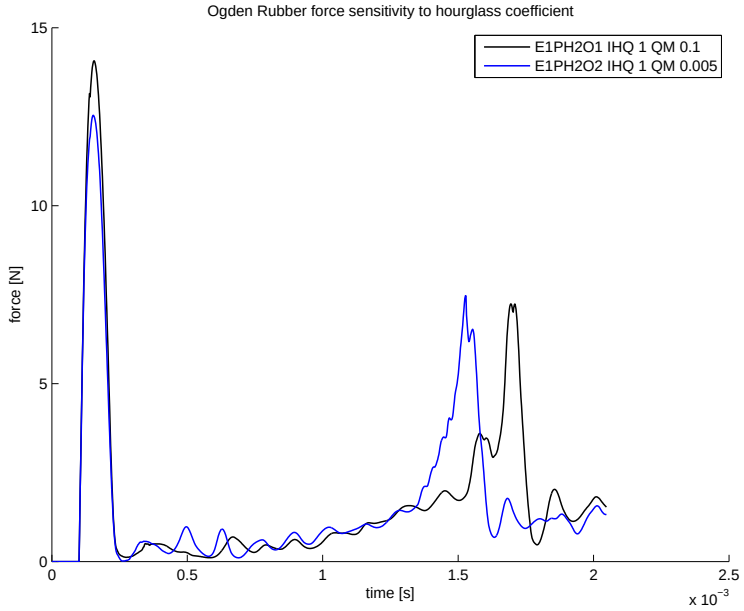

Figure D.2: Hourglass formulation study

The hourglass coefficient have been varied from visible hourglassing modes in the simulation to no visible hourglassing modes. When there are no hourglass modes the hourglass energy is higher than the 10

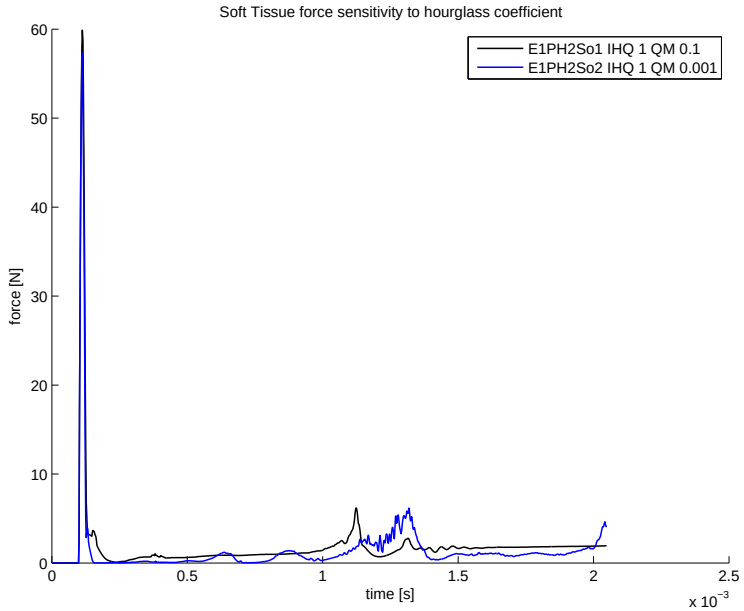

Figure D.3: Hourglass formulation study

Acording to figure D.3 there is little influence of hourglass coefficient to the force in the indentor with the Soft Tissue. It still does vary a bit in the end were the comparison is going to be made but it is at least in the right ballpark.

E Frictional sensitivity analysis

The sensitivity of the forces with respect to the friction needs to be investigated in order to see if frictional formulation is needed or not. If the force is very sensitive to the friction coefficients, care has to be taken in choosing the correct values.

E.1 Calibration

In these tests the Ogden model is used with $\mu = 40$, $\alpha = 20$ and a viscoelastic contribution by a one term prony serie with coefficients $\beta_1 = 310$ and $G_1 = 3000$. The engineering strain rate is 100/s. Further the dimensions of the specimen are radius 5 mm and length 3 mm.

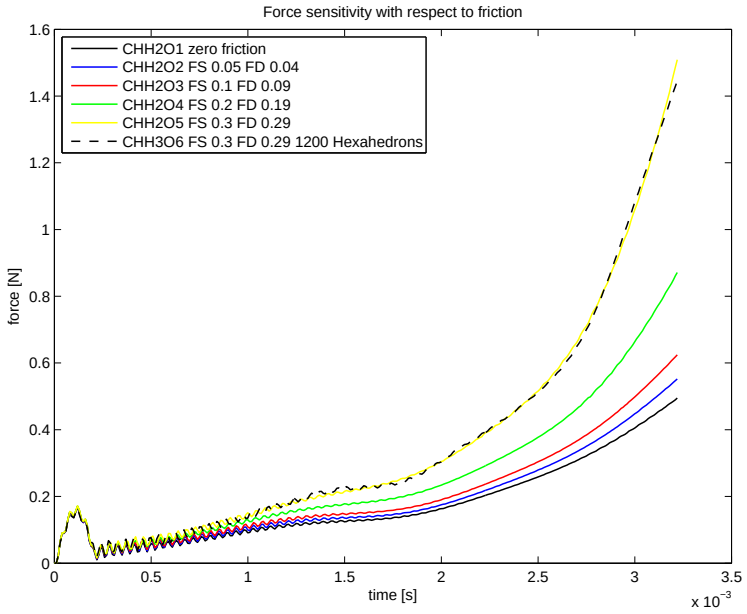

Figure E.1: Frictional sensitivity analysis. Ogden model with viscoelastic contribution

According to figure E.1 it can be concluded that for the ogden model with viscoelastic contribution the friction has almost zero influence at small strains. At larger strains the curves deviate and the force become more and more sensitive to friction with increasing values of the coefficients. According to Bjork steel on steel has friction coefficients FS=0.18 and FD=0.14. It is reasonable to assume that WAT on nylon platens has lower values of friction coefficients. According to Bjork steel on steel with lubricated surfaces has friction coefficients FS=0.1 and FD =0.05. It is reasonable to assume that these values are very close to the values of WAT on nylon platens and since the sensitivity is lower when FS and FD are lower it becomes less critical to establish exact values on the friction coefficients hence FS=0.1 and FD=0.05 are going to be used further on for the WAT on nylon platens. In figure E.1 the black dashed line corresponds to an analysis with higher mesh density and it can be concluded that the mesh density used is sufficient. This was done since the stressfield obviously changes as the friction coefficient is increased resulting in a more nonlinear stressfield.

F Stress sensitivity to bulk modulus or poissons ratio

In order to save analysis time it is reasonable to check the sensitivity of stress to the value of the bulk modulus since a lowering of the bulk modulus reduces simulation time.

F.1 Evaluation 2

The simulation times for the three tests in evaluation 2 are relatively slow, 015 s, 1.5 s and 15 s. The last two would take a considerable amount of time to calculate with the explicit method therefore the implicit method is used for all three. Further since the bulk modulus is relatively high the simulation time is also long for the implicit method. A sensitivity test at 0.015 s simulation time with the explicit method has been performed with various poissons ratios and bulk modulus' including the correct one, for all three material models. The calculations have been performed with elform=3 in order to eliminate hourglassing. The argument is since this sensitivity test is performed at a faster simulation time it would be sufficient to validate the use of a lower poissons ratio or bulk modulus if there is low enough sensitivity of poissons ratio or bulk modulus to the shear stress. This since this faster simulation will only increase inertial effects and stress due to strain rate dependency which would be a more severe case than the slower ones.

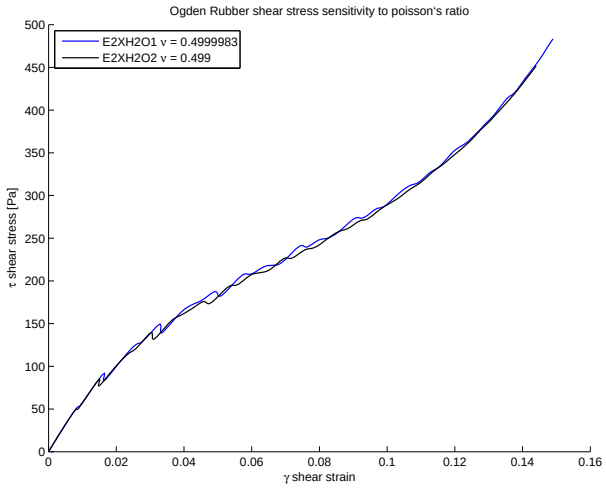

Figure F.1: Mesh density 200 hexahedrons, elform = 3

As can be seen in figure F.1 it is assumed safe to use a poissons ratio of 0.499 for the three tests in evaluation 2.

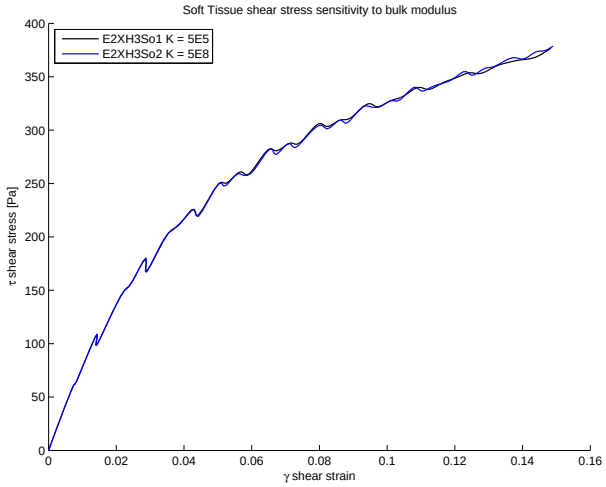

Figure F.2: Mesh density 600 hexahedrons, elform = 1

As can be seen in figure F.2 it is assumed safe to use a bulk modulus between 5E5 to 5E8 for the three tests in evaluation 2.

G List of simulations

Below follows a brief description of the various simulations performed on the Calibration, Evaluation 1 and Evaluation 2. A table of simulations is included in appendix amongst the material keyword cards used in LS-DYNA.

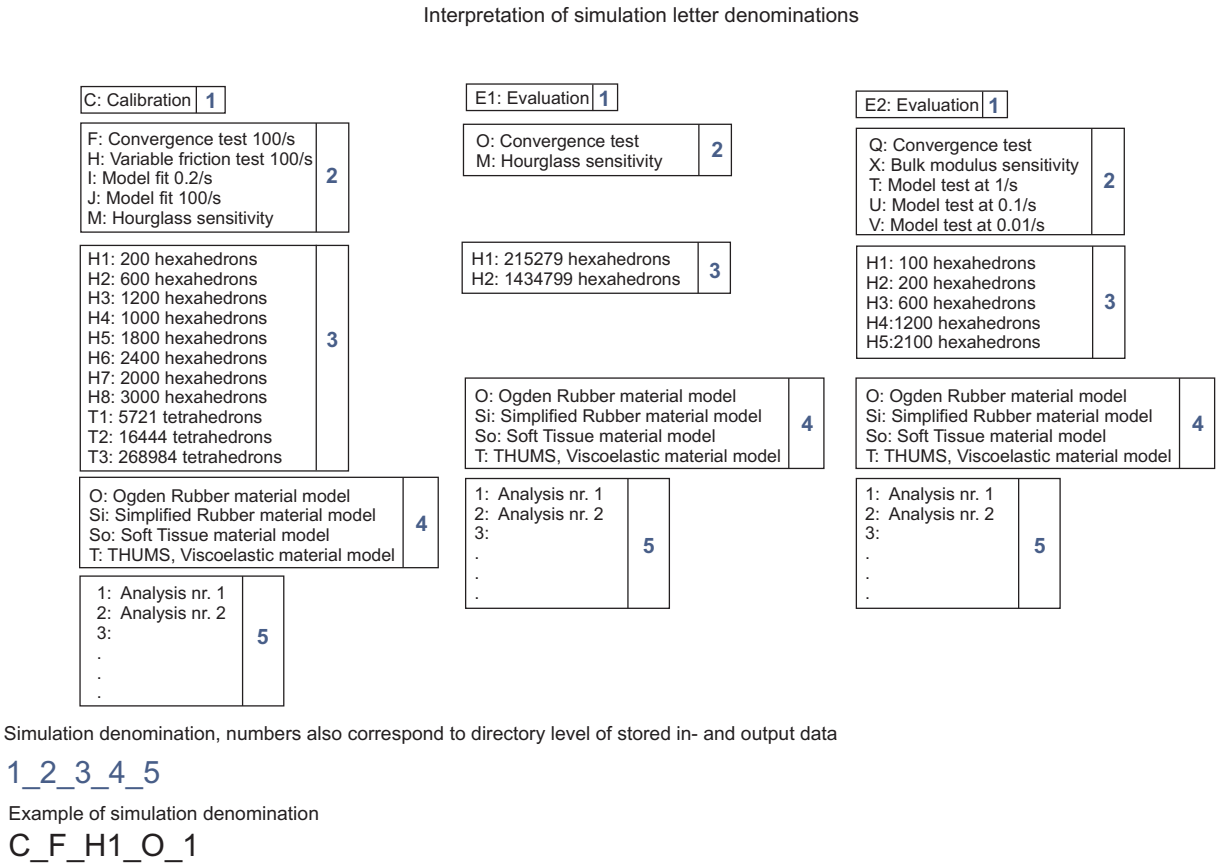

Figure G.1: Simulation denominations and roadmap of directory structure for storing indata and outdata

Denomination	Varied Parameters	Value of varied parameter
Calibration		
CFH1O1	Mesh density	200 elements
CFH2O1	Mesh density	600 elements
CFH3O1	Mesh density	1200 elements
CFH1Si1	Mesh density	200 elements
CFH2Si1	Mesh density	600 elements
CFH3Si1	Mesh density	1200 elements
CFH7Si1	Mesh density	2000 elements
CFH8Si1	Mesh density	3000 elements
CFH1So1	Mesh density	200 elements
CFH2So1	Mesh density	600 elements
CHH2O1	FS, FD	FS 0 FD 0
CHH2O2	FS, FD	FS 0.05 FD 0.05
CHH2O3	FS, FD	FS 0.1 FD 0.1
CHH2O4	FS, FD	FS 0.3 FD 0.3
CHH2O5	FS, FD	FS 0.2 FD 0.2
CHH3O6	FS, FD	FS 0.3 FD 0.3
CIH5O1	shear modulus μ_1	$\alpha_1 = 20, \mu_1 = 40, \rho = 920, G_1 = 0, \beta_1 = 0, \nu = 0.4999983$
CIH5Si1	Input curves	$K = 0.5E9, SW = ST = SL = 1, TBID = 5000$
CIH5So1	C_1, C_2	$XK = 0.5E9, S_1 = 0, G_1 = 0$
CJH2O1	shear modulus μ_1, G_1, β_1	$\alpha_1 = 20, \mu_1 = 30, \rho = 920, G_1 = 3000, \beta_1 = 310, \nu = 0.4999983$
CJH8Si1	Input curves	$K = 0.5E9, SW = ST = SL = 1, TBID = 5000$
CJH2So1	C_1, C_2, S_1, G_1	$XK = 0.5E9, S_1 = 0.00322, G_1 = 10$
CMH2O9	IHQ, QM, elform	no hourglass formulation, elform=3
CMH2O11	IHQ, QM, elform	IHQ=1, QM=0.1, elform=1
CMH2O12	IHQ, QM, elform	IHQ=1, QM=0.05, elform=1

Table G.1: Table simulations for Calibration

Denomination	Varied Parameters	Value of varied parameter
Evaluation 1		
E1OH1O1	Mesh density	215279 elements
E1OH2O1	Mesh density	1434799 elements
E1OH1So1	Mesh density	215279 elements
E1OH2So1	Mesh density	1434799 elements
E1PH1O1	IHQ, QM	IHQ=1, QM=0.1
E1PH1O2	IHQ, QM	IHQ=1, QM=0.005
E1PH1So1	IHQ, QM	IHQ=1, QM=0.1
E1PH1So2	IHQ, QM	IHQ=1, QM=0.005

Table G.2: Table simulations for Evaluation 1

Denomination	Varied Parameters	Value of varied parameter
Evaluation 2		
E2QH1O1	Mesh density	100 elements
E2QH2O1	Mesh density	200 elements
E2QH3O1	Mesh density	600 elements
E2QH3Si1	Mesh density	600 elements
E2QH4Si1	Mesh density	1200 elements
E2QH5Si1	Mesh density	2100 elements
E2QH2So1	Mesh density	200 elements
E2QH3So1	Mesh density	600 elements
E2QH2T1	Mesh density	200 elements
E2QH3T1	Mesh density	600 elements
E2XH2O1	ν	$\nu = 0.4999983$
E2XH2O2	ν	$\nu = 0.499$
E2XH3So1	K	K=5E5
E2XH3So2	K	K=5E8
E2TH2O1	none	evaluation of already existing values
E2TH2So1	none	evaluation of already existing values
E2TH2T1	none	evaluation of already existing values
E2UH2O1	none	evaluation of already existing values
E2UH2So1	none	evaluation of already existing values
E2UH2T1	none	evaluation of already existing values
E2VH2O1	none	evaluation of already existing values
E2VH2So1	none	evaluation of already existing values
E2VH2T1	none	evaluation of already existing values

Table G.3: Table simulations for Evaluation 2

H Material Keycards

The material keyword cards are presented for the material models used in the simulations. The keyword cards are presented with the final parameter values after the calibration experiment. The Simplified Rubber model has TBID 5000 as input curves which corresponds to the curves in figure 4.13.

```
*MAT_OGDEN_RUBBER
$#     mid        ro        pr         n        nv         g      sigf
         2       920 0.4999983         0         6     0.000     0.000
$#     mu1       mu2       mu3       mu4       mu5       mu6       mu7       mu8
          30     0.000     0.000     0.000     0.000     0.000     0.000     0.000
$#  alpha1    alpha2    alpha3    alpha4    alpha5    alpha6    alpha7    alpha8
 20.000000     0.000     0.000     0.000     0.000     0.000     0.000     0.000
$#      Gi        Bi
       3E3       310
*MAT_SOFT_TISSUE_VISCO_TITLE
softtissue
$#     mid        ro        c1        c2        c3        c4        c5
         1 920.00000       100       100     0.000     0.000     0.000
$#      xk      xlam      fang     xlam0
 5.0000E+8 10.000000     0.000     0.000
$#    aopt        ax        ay        az        bx        by        bz
  2.000000     0.000  1.000000     0.000     0.000     0.000  1.000000
$#     la1       la2       la3      macf
     0.000     0.000     0.000         1
$#      s1        s2        s3        s4        s5        s6
         10     0.000     0.000     0.000     0.000     0.000
$#      t1        t2        t3        t4        t5        t6
   0.00322     0.000     0.000     0.000     0.000     0.000
*MAT_SIMPLIFIED_RUBBER/FOAM_TITLE
simplified
$#     mid        ro         k        mu         g      sigf       ref     prten
         3 920.00000 5.0000E+8     0.000     0.000     0.000     0.000     0.000
$#     sgl        sw        st   lc/tbid   tension     rtype    avgopt   pr/beta
  1.000000  1.000000  1.000000      5000  1.000000  1.000000     0.000     0.000
*MAT_VISCOELASTIC
$#     mid        ro      bulk        g0        gi      beta
         4      1200 2.2960E+6 3.5060E+5 1.1690E+5 100.00000
```

Figure H.1: Material keyword cards used in LS DYNA [21]